August 2020

Experimental Study on Side Resistance of Energy Pile in Winter-mode Operation

Te-An Wang
University of Wisconsin-Milwaukee

EXPERIMENTAL STUDY ON SIDE RESISTANCE OF ENERGY PILE IN WINTER-MODE OPERATION

by

Te-An Wang

A Dissertation Submitted in

Partial Fulfillment of the

Requirements for the Degree of

Doctor of Philosophy

in Engineering

at

The University of Wisconsin-Milwaukee

August 2020

ABSTRACT

EXPERIMENTAL STUDY ON SIDE RESISTANCE OF ENERGY PILE IN WINTER-MODE OPERATION

by

Te-An Wang

The University of Wisconsin-Milwaukee, 2020

Under the Supervision of Professor Helwany

In the present work, the side resistance of an energy pile subjected to a significant number of thermal cycles in saturated Kaolin clay was investigated through small-scale pile tests, direct shear tests, and triaxial tests. Before applying compressive load, relative shearing displacement, or deviator stress, up to 36 cooling/heating cycles were performed on the soil-foundation interface and soil. The thermal cycle was below the average ground temperature in temperate zones to simulate the winter-mode operation. In small-scale pile tests, the long-term behavior of the pile was observed in terms of temperature distribution and pore water pressure in soil, and a 15% relative settlement criterion was adopted to define the failure load. In direct shear tests, failure is taken to correspond to

the maximum shear stress attained, or shear stress at 10% relative shear displacement. In triaxial tests, failure is taken to correspond to the maximum deviator stress attained, or deviator stress at 15% axial strain. If soil is subjected to long-term temperature cycling, however, time plays an essential role in affecting mechanical performances. Therefore, under ambient temperature, a series of tests were carried out in direct shear tests and triaxial tests to analyze the effect of time of which is referred to as an aging influence. The results show that the pile subjected to temperature cycling has weaker side resistance than the isothermal pile tested at room temperature due to soil erosion by condensate water, but this is not the case for the soil-foundation interface in the direct shear test. In direct shear tests and triaxial tests, although the heating/cooling cycles induced the clay to have a significant contraction, the elapsed time of temperature cycling is the main factor for increasing the resistance to shear deformation.

TABLE OF CONTENTS

LIST OF FIGURES

LIST OF TABLES

Chapter 1

Thermo-Mechanical Behavior of Energy Pile and Research Plan

1 Introduction

1.1 Motivation

Energy piles or heat exchanger piles have initially been developed in Austria in the 1980s, and they are the structural support element and an innovative way to use geothermal energy [1]. Subsurface geothermal offers a carbon-free and sustainable form of energy to homes and office buildings by connecting deep foundations with ground source heat pump systems (GSHPs).

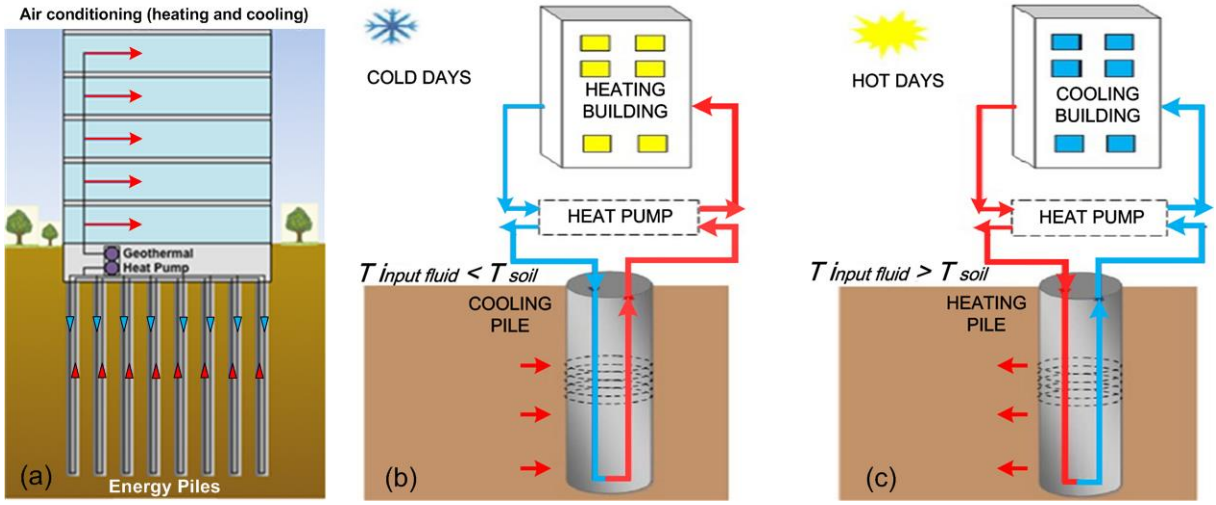

Figure 1-1: Schematic of energy piles operations: (a) space heating/cooling, (b) heat energy extraction and (c) heat energy storage

With combined geothermal heat pumps, heat energy is fed into and withdrawn from the ground as shown in Figure 1-1. Compared to traditional systems using fossil fuels or

electricity, this technique reduces heating energy by 20–40% and cooling costs by 30–50% [2]. The temperature range imposed by energy foundations exploitation is falling between 4°C to 30°C [3], and the operation creates differential temperatures between the pile and the soil around the pile.

Faizal et al. (2016) [4] monitored a fall-scale energy pile in Melbourne, Australia for 480 hours. Their experiment used an intermittent chiller to cool circulate water at 5°C for simulating the heating operation during cold days. They noted the operation of energy pile had the pile and surrounding soils undergo temperature fluctuation as shown in Figure 1-2.

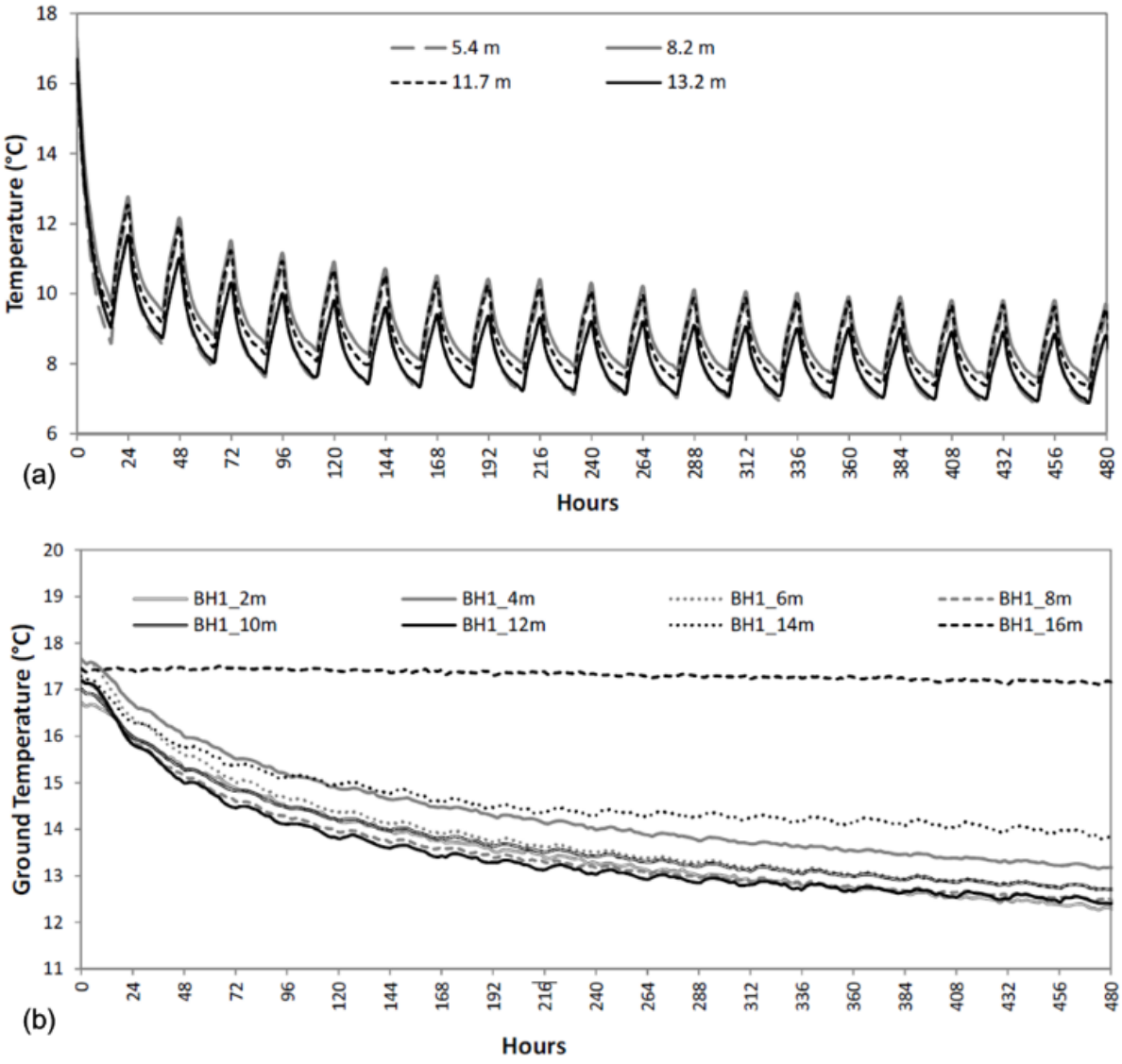

Figure 1-2: Monitor of the full-scale energy pile in Melbourne, Australia: (a) Pile transient temperature and (b) ground temperatures [4]

The heat energy extraction/storage changes the temperature of piles and ground therefore posing safety concerns of geothermal structures, but due to the lack of design

standards, the implementation of energy foundations is not consistent across countries.

The investigation regarding the thermo-mechanical behavior of energy piles can be mainly divided into two categories: (1) temperature effects on soil behavior and (2) shear stress mobilization/relaxation at the soil-pile interface due to thermo-elastic pile deformation. In the first one, soil behavior is affected by thermal history imposed by the energy pile. For example, changes in temperature can arouse the microstructure of cohesive soil to reorient [5], changes in volume [6, 7], and excess pore water pressure [8] which thus affect the shear strength of the soil. In the latter category, thermally-induced pile deformation gives rise to change the internal stress along the foundation [9] as show in Figure 1-3. The intensity of thermally-induced strain depends on constraints at the ends of the pile [9] and the type of surrounding soil [10]. It may result in repeated cyclic shear straining, which can potentially reduce axial capacity of energy pile.

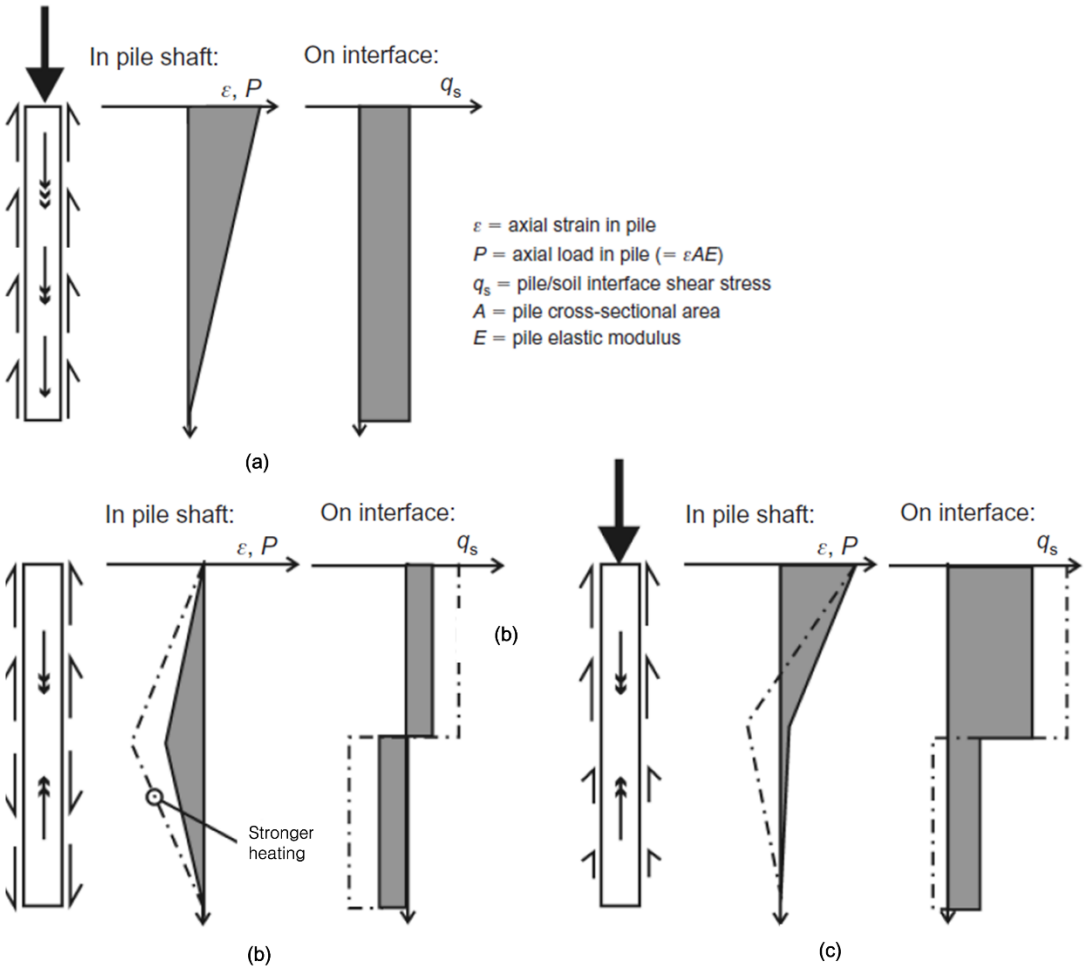

Figure 1-3: Mechanism for response of pile to thermal loading during cold days: (a) load only; (b) cooling only; (c) combined load and cooling [9]

Although many experimental studies have been carried out to investigate the thermo-mechanical behavior of soils, few investigations focused on evaluating the effects of heating/cooling cycles. In terms of temperature effect on soil shear strength, the thermally induced volume changes have a complex impact on the soil shear strength that thermal

expansion under undrained heating leads to a reduction of soil strength, while the thermal contraction under drained heating hardens the soil and increases the shear strength [7, 11-13]. Still, the time-dependent behavior of soil skeleton (aging) also influences thermal consolidation phenomena, but it drew little attention in investigations. Schmertmann (1991) [14] presents examples of improvement in drained creep movements associated with aging, with the driving energy supplied by the in situ effective stresses, tend to disperse complicated structure in fine-grained soils. He indicated that this dispersion then leads to an increased basic frictional mobilization capability of the soil. Perhaps as parts of the structural fabric of the soil stiffen due to the dispersion under the drained conditions during aging, the stresses arch to these stiffer parts. Or the dispersive movements may occur primarily in the weaker, softer parts of the fabric and cause an arching stress transfer to the stiffer parts. Either way, this arching occurs internally at the particulate level with the overall, average effective stress remaining constant. The stiffer parts of the fabric probably also have greater strength, at least statistically, thus increasing the overall effective stress stiffness and strength of the soil [14].

Over the years, various laboratory experiments have been conducted to study the

side resistance of energy piles, the experiments include direct shear tests, 1-g model pile tests, and increased g-levels model pile tests in the centrifuge. A summary of previous experimental studies investigating temperature effects on side resistance of energy pile is provided in Table 1-1. Donna et al. (2015) [15] presented the direct shear test results on the response of both sand/clay-concrete interface at elevated temperatures. They noted no change in shear resistance with sand but an increase in shear resistance with clay. Similarly, Yazdani et al. (2019) [16] performed similar direct shear tests using normally consolidated (NC) Kaolin, and they observed an increase in shear resistance at increased temperature and heating/cooling cycles. However, Yavari et al. (2016)[17] had different results of Kaolin-concrete interface resistance at elevated temperatures and heating/cooling cycles through direct shear tests. Their observation indicates that the effect of temperature on the shear strength of clay-concrete interface is negligible. In small-scale models tested under 1-g or at increased g-level, the temperature ranges that have been studied by other authors are usually above room temperature. Their results reveal the side resistance of pile increases on heating or cyclic thermal load above room temperature [18-21].

It can be found that most references have focused on the side resistances of energy piles and mechanical behaviors of surrounding soils during summer operation. However energy piles can be used for heating and/or cooling buildings of all sizes, as well as snow melting systems for road pavements and bridge decks, but few works investigate the thermo-mechanical behaviors of energy pile at decreased temperature or winter operation.

Table 1-1: Summary of laboratory experimental studies investigating the temperature effect on side resistance of energy piles

Study	Author	Soil type	Pile type	Thermal load (°C)	Remarks
Direct shear test	Donna et al. (2015) [15]	(1) Saturated Bernasconi grey quartz sand: D_{50} = 0.5 mm (2) Saturated Illite clay: D_{50} = 0.002 mm	Concrete surface	20 → 60	(1) Sand-concrete: No change in shear strength (2) Clay-concrete: Increase in shear strength with heating
	Yavari et al. (2016) [17]	Saturated Kaolin clay: e = 1.35 LL = 57% PL = 33%	Concrete surface	20 → 40 20 → 40 → 20 20 → 40 → 5	No change in shear strength
	Yazdani et	Saturated Kaolin	Concrete	24 → 34	OCR = 1: Increase in

Study	Author	Soil type	Pile type	Thermal load (°C)	Remarks
	al. (2019) [16]	clay: D_{50} = 0.0026 mm LL = 45% PL = 25% OCR = 1, 2, 5	surface	24 ⇆ 34 (10 cycles)	shear strength with heating and cyclic thermal load OCR > 1: Decrease in shear strength with heating and cyclic thermal load
1-g model pile test	Huang et al. (2018) [20]	Saturated sandy soil: D_{50} = 0.34 mm	Aluminum tube sealed at the bottom OD = 49.98 mm End bearing: Yes	20 → 50 20 → 35 20 → 15 20 → 5	Bearing capacity of pile increases with heating and decreases with cooling
	Yazdani (2019) [16]	Saturated Kaolin clay: D_{50} = 0.0026 mm LL = 45% PL = 25%	Stainless tube coated with concrete OD = 19 mm End bearing: No	24 → 34 24 ⇆ 34 (up to 40 cycles)	Side resistance increases with heating and cyclic thermal load
Centrifuge-scale pile test	McCartney (2011) [22]	Silt: ω = 13.6% r_d = 17.2 kN/m^3	Concrete tube seal at the bottom OD = 76.2 mm End bearing: Yes	15 15 → 50 15 → 50 → 20	g-level: 24 Side resistance increases with heating and cyclic thermal load
	Ng et al. (2014) [18]	Saturated Toyoura sand: D_{50} = 0.17 mm	Aluminum tube sealed at the bottom OD = 22 mm	22 → 37 22 → 52	g-level: 40 Side resistance increases with heating but at a

Study	Author	Soil type	Pile type	Thermal load (°C)	Remarks
			End bearing: Yes		reducing rate

1.2 Objectives

This study presents the thermo-mechanical behavior of energy pile embedded in NC Kaolin. The energy pile was in GSHP operating temperature pattern and particularly during cold days that make ground behave as a heat resource. The goal is to investigate: (1) changes in side resistance between the soil and the pile at decreased temperatures; (2) soils deformation under cyclic thermal loading; (3) the effect of cyclic thermal load on soil shear strength; and (4) the influence of time on soils thermomechanical behavior.

1.3 Approach

Seasonal ground temperatures remain at around 15°C from 10 m to 50 m below ground surface (see Figure 1-4) while most energy piles have temperature ranges of 4°C to 20°C.

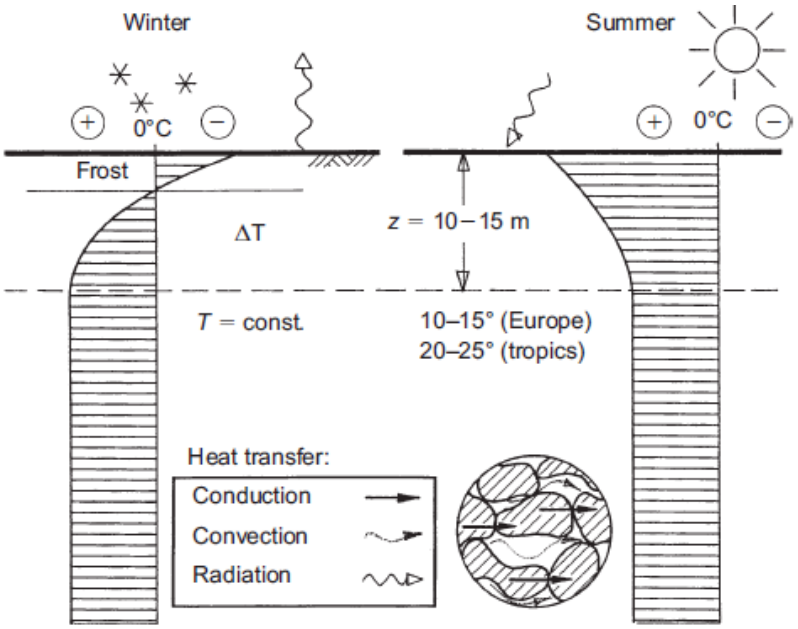

Figure 1-4: Heat transfer and geothermal conditions for deep foundations. Ground temperature tends to be constant after a depth of about 10 m to 15 m [1]

During winter operation, soil behaves as a heat source. Absorbing heat energy from soil reduces the temperature of piles and the surrounding soil. Therefore, this research considers T = 15°C as the average temperature at a shallow depth where the energy pile is installed, and T = 4°C as the lowest temperature that soil-pile interface can reach.

Water is the soil component most affected by temperature changes and can exist in any of its three phases: ice, liquid water, and water vapor. In particular, liquid water can have complex forms as a result of its interaction with the soil. Temperature plays a critical role not only in determining the phase distribution, but also influencing water properties,

water movement, and the degree of its interaction with solid soil particles [23]. When soil freezes, water is drawn to the freezing front, thereby altering the soil's thermal properties in both the frozen and unfrozen zones. Therefore, to simplify the variables this research focused on the soil's properties in unfrozen zone ($T > 0°C$).

Please note that the temperature in the absorber pipes in the geothermal extraction usually avoids falling below 0 to 5°C for the economic reasons [1]. However, in the extreme cases, the temperature of the thermal fluid can possibly fall below the suggested temperatures (0 to 5°C) [1, 9, 24]. This research aimed to cover the temperature range of extreme extraction, therefore 4°C is considered as the lowest temperature that can be encountered in Kaolin and at Kaolin-pile interface.

To investigate the effects of extreme (undrained) and moderate (drained) thermal cycling operations on side resistance, three small-scale pile tests and four groups of soil-concrete direct shear tests are employed herein. Effects of thermal cyclic loads on the engineering behavior of soil have been investigated through slow direct shear tests and slow consolidated drained (CD) triaxial tests. Because a significant number of thermal cycles takes very long time, soils subjected to these thermal cyclic loads are also

subjected to time effect. To investigate the impact of time (referred to as aging herein) on the clay under thermal cycling conditions, several tests with different aging times were performed on isothermal samples. Testing materials, experimental programs, and test results will be described in detail in the following section.

Chapter 2

Soil Physical Properties and Sample Preparations

2 Materials

2.1 Soil Properties

The soil used in this study is a reconstituted Kaolin HC-77 with a specific gravity of 2.63. This soil is commercially available as a powder. Table 2-1 shows the soil's basic physical properties. Preparation of soil specimens begins with a slurry (as shown in Figure 2-1) to obtain homogeneous and fully saturated specimens.

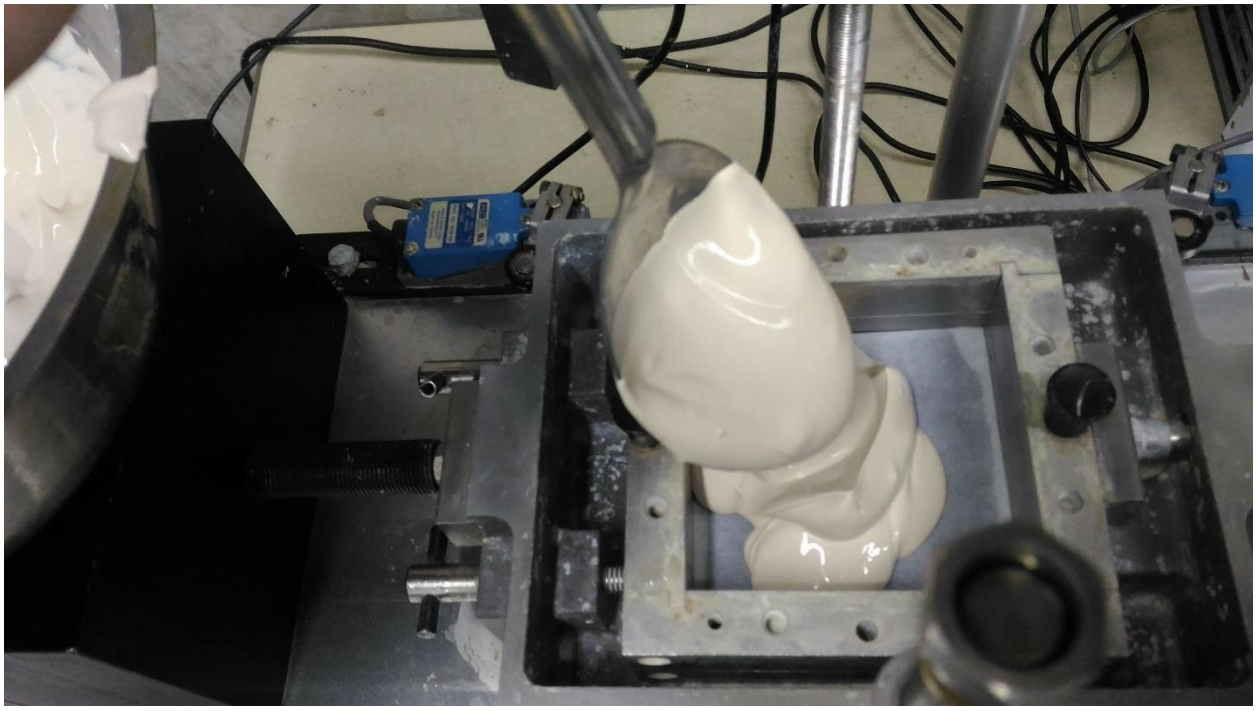

Figure 2-1: Kaolin slurry

The slurry is a mixture of air-dried Kaolin powder and water with a water content of

70% that is nearly twice the liquid limit of Kaolin. The slurry was then normally consolidated at 25°C through several steps of loading up to 100 kPa. At the end of the consolidation phase, the clay specimen has the characteristics listed in Table 2-1.

Table 2-1: Summary of BURGESS HC77 Kaolin

Property	Value/Classification
USCS Classification	CL
Specific Gravity	2.63
Liquid limit (%)	35
Plastic limit (%)	19
D_{10} (mm)	< 0.0009
D_{30} (mm)	0.0015
D_{60} (mm)	0.0034
Afte 100-kPa consolidation	
Total unit weight (kN/m^3)	≈17.28
Initial moisture content (%)	≈34.42
Initial void ratio, *e*	≈0.94
Initial saturation degree, S	≈0.96

2.2 Concrete material

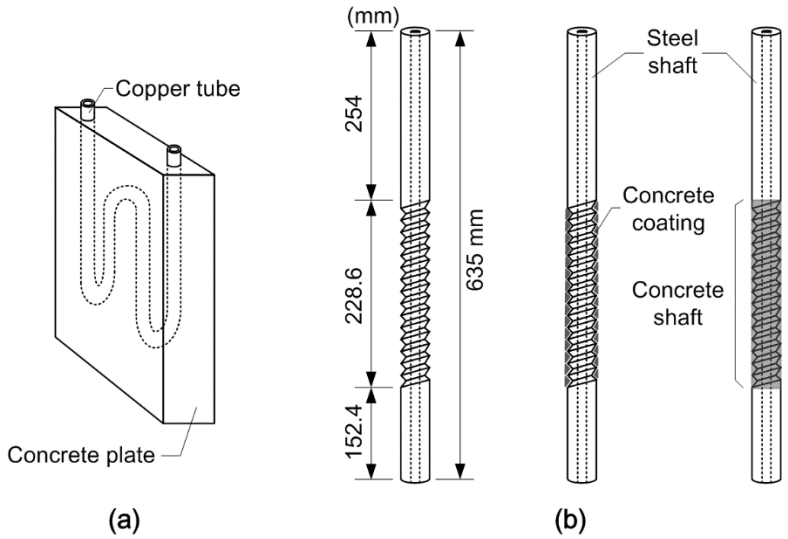

Figure 2-2: Schematic view of (a) concrete plate; (b) model pile

The concrete plate for the interface shear tests and the concrete coatings of the model pile for the pile tests are made of cement, sand, and water in ratio of 1:1:0.3. Schematic of the concrete plate and the pile are shown in as shown in Figure 2-2. Dimensions of the concrete plate are 152.4 mm (L) × 152.4 mm (W) × 25.4 mm (H). Inside of the slab, a flexible copper tube (OD: 9.52 mm) that embedded as a part of the heating/cooling system as shown in Figure 2-3.

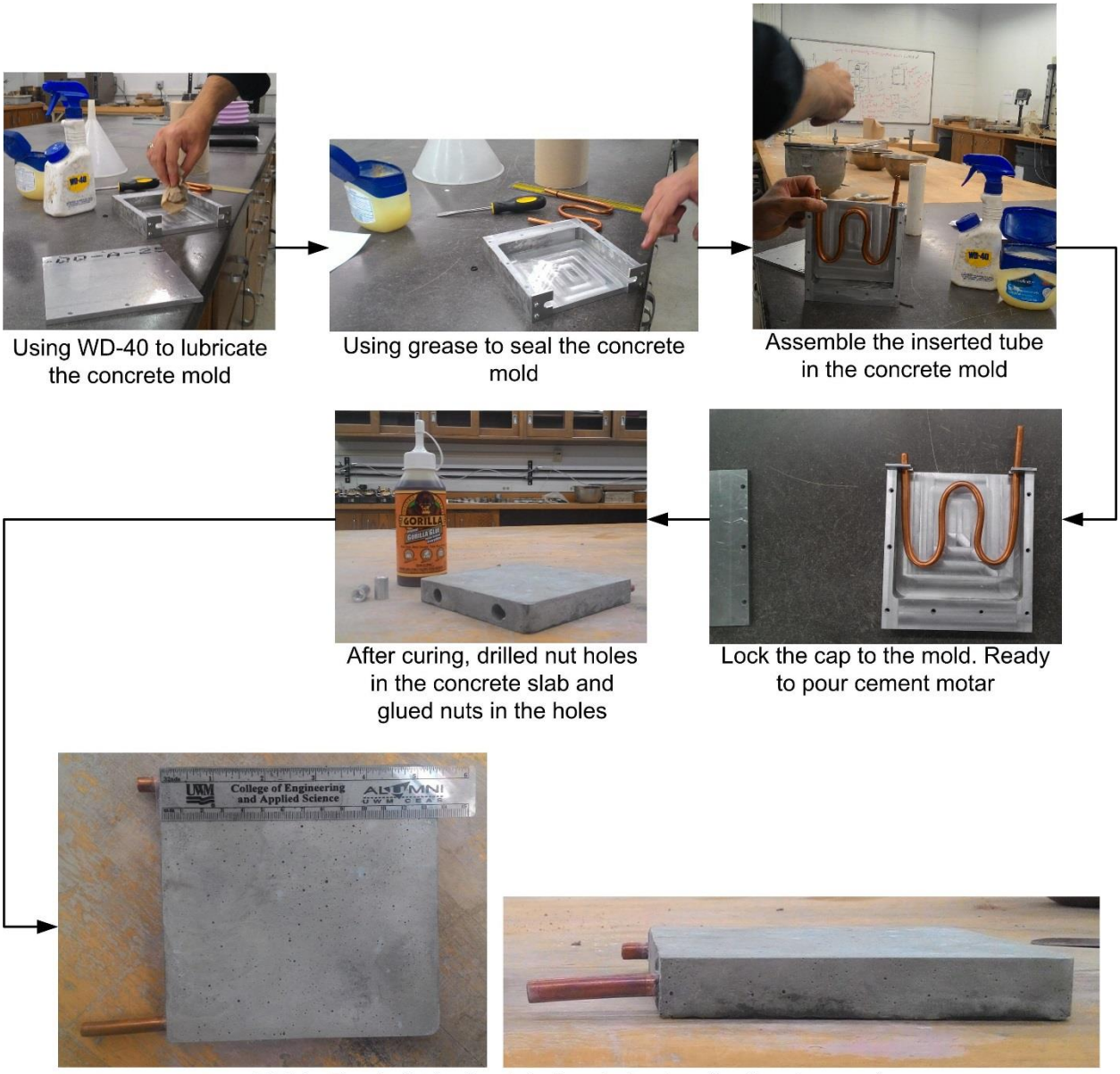

Figure 2-3: Concrete plate implemented with heating/cooling pipe

In pile tests, the pile is made of a stainless steel circular tube with dimensions of 635 mm (L), 22.225 mm (OD), and 18.653 mm (ID). From the length of 254 mm to 482.6 mm,

the pile surface was threaded and coated with concrete so that the concrete coating can firmly attach to the steel surface without changing the outer diameter of the pile as shown in Figure 2-4.

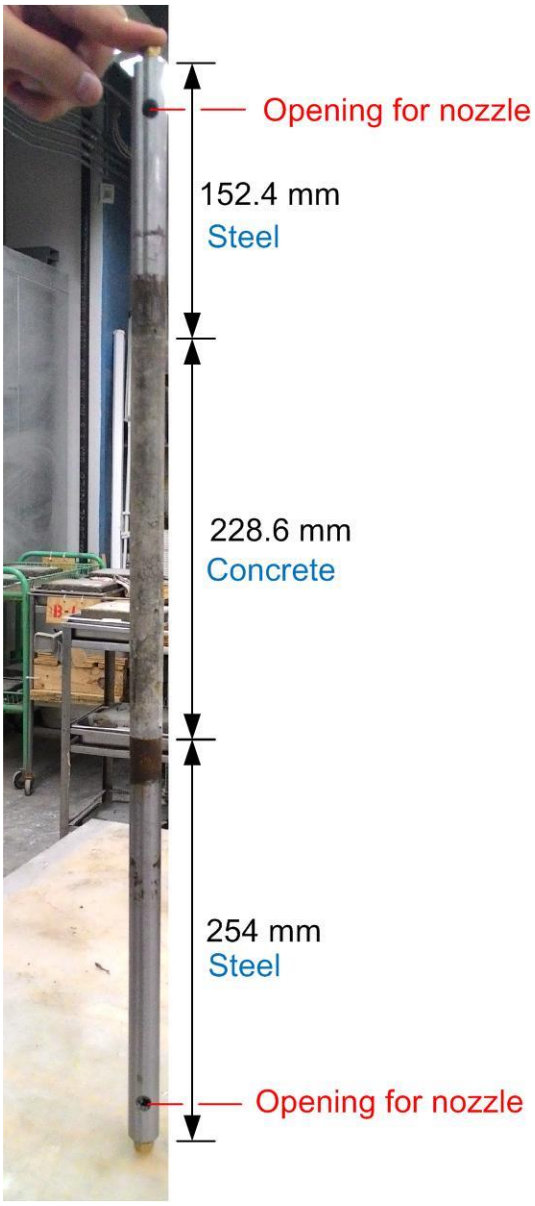

Figure 2-4: Model pile

Chapter 3

Test Methods and Experiment Layouts

3 Equipment Setup

3.1 Small-Scale Pile Test

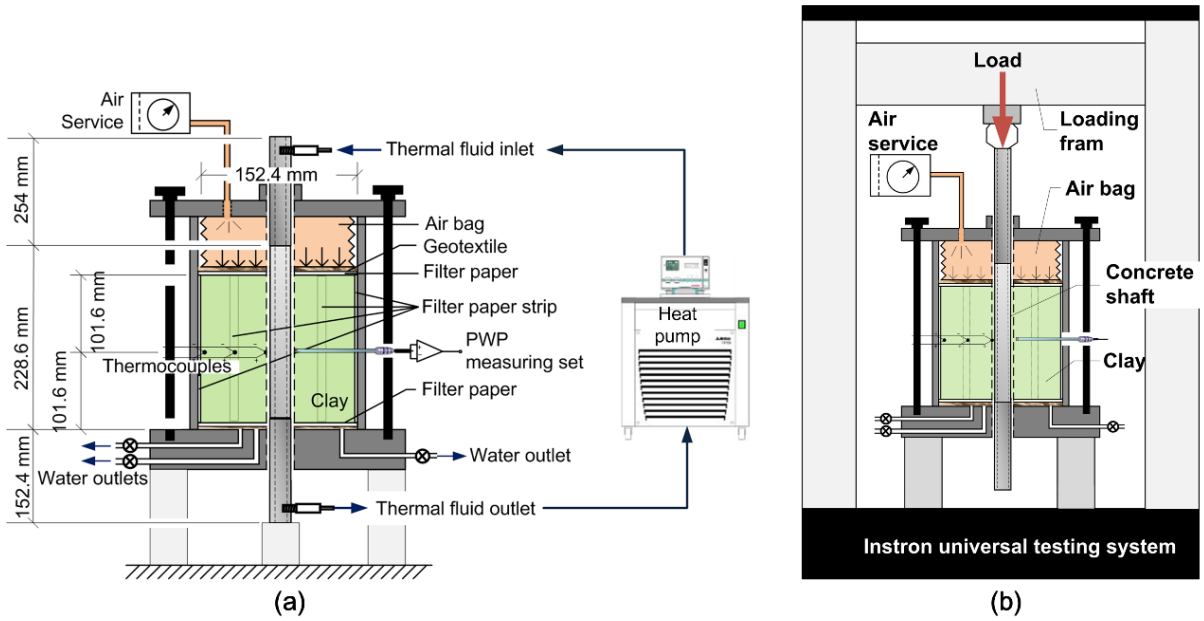

Figure 3-1: Schematic of pile test (a) during sample preparation (not on scale); (b) during loading phase

Figure 3-1 shows a schematic diagram of a model-scale pile test. In order to carry out the load-controlled test, an Instron Universal Testing System is employed. Because the pile self-weight may causes settlement, a bottom constraint was used for the pile during the consolidation and temperature cycling stages. The bottom constraint is removed during compressive loading stages, so the pile can slide freely through the opening at the bottom of the compression chamber. Sample was assembled in a

lubricated, heavy-duty acrylic compression chamber with dimensions of 304.8 mm (Depth) and 152.4 mm (ID). The clay had a depth of 203.2 mm after consolidation, which was 25.4 mm shorter than the concrete shaft. The steel shaft was lubricated so that the frictional resistance was only mobilized between the concrete surface and the surrounding clay. An equivalent vertical effective stress of 100 kPa was applied at the top surface of the clay using a doughnut-shaped airbag (OD: 150 mm) to simulate the in situ stresses at a given depth, z (see Figure 3-2)

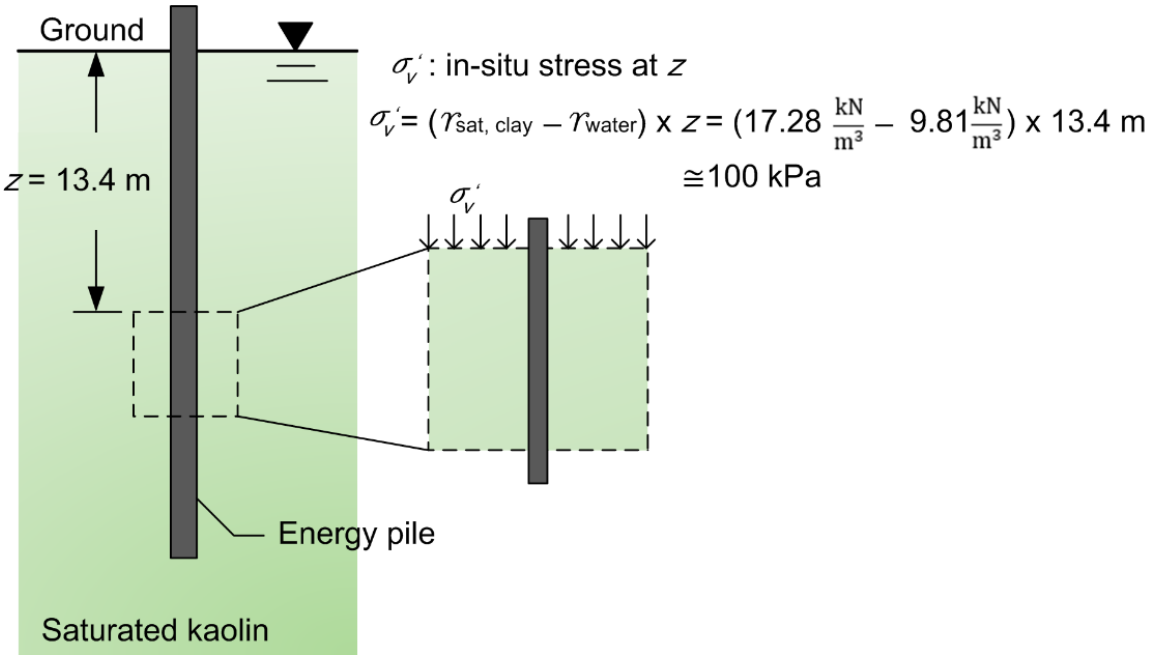

Figure 3-2: Pile subsection analysis under simplified conditions

A heat pump with a working temperature range of -50 to +200°C is used to apply

heat cycles on the pile. An electronic pore water pressure transducer is used to measure the pore water pressure during the application of heat cycles. As shown in Figure 3-1(a), three K-type thermocouples and a pore water pressure transducer were positioned at the middle height of the soil. To minimize soil disturbance, the pore pressure transducer is attached to a long probe as shown in Figure 3-3. The distance between the probe tip and pile surface was 3 mm. The probe consists of a 5.08 mm diameter bronze porous stone (thickness: 6.35 mm) glued to a tiny copper pipe (OD: 3.175 mm; ID: 1.651 mm). The calibration results of the PWP measuring device are shown in Figure 3-4. The thermocouples were at three distances from pile surface: 3, 33, and 63 mm, respectively, to measure temperature distribution in the soil during the heat cycling as presented in Figure 3-5.

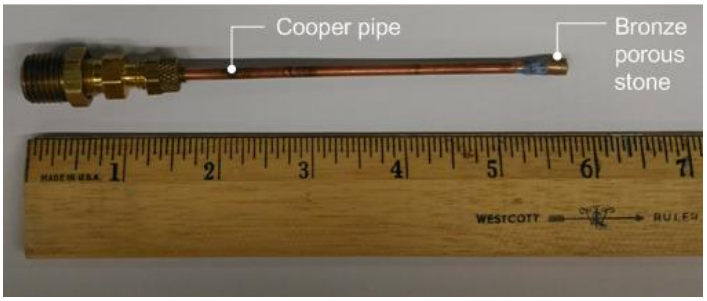

Figure 3-3: Pore water pressure (PWP) probe

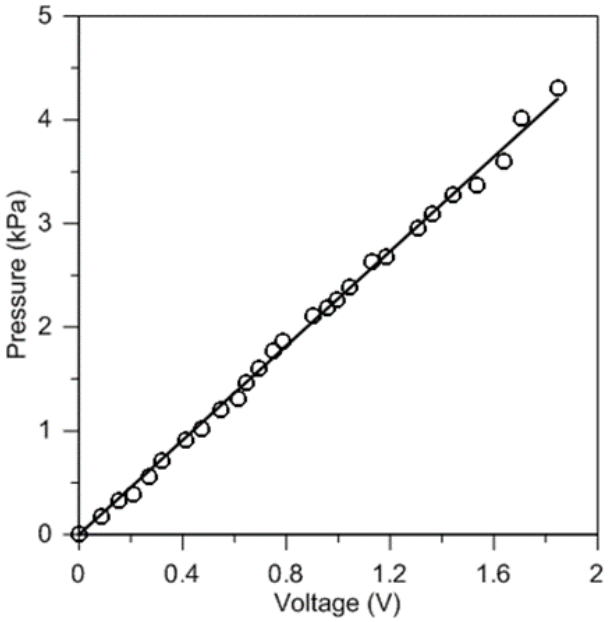

Figure 3-4: Calibration of the pore water pressure transducer with probe

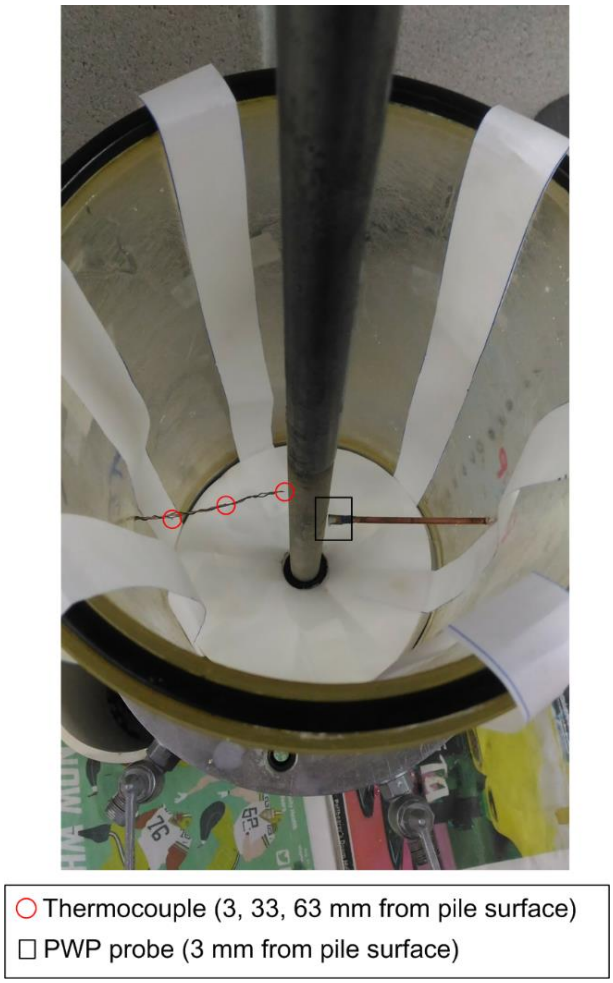

Figure 3-5: Arrangement of thermocouples and PWP probe

3.2 Slow Soil-Concrete Interface Direct shear Test

Figure 3-6 is a schematic presentation of the modified direct shear test apparatus for testing soil-concrete interface shear strength. The upper half of the direct shear box contained the normally consolidated Kaolin with dimensions of: 101.6 mm (L), 101.6 mm

(W), and 19.4 mm (H).

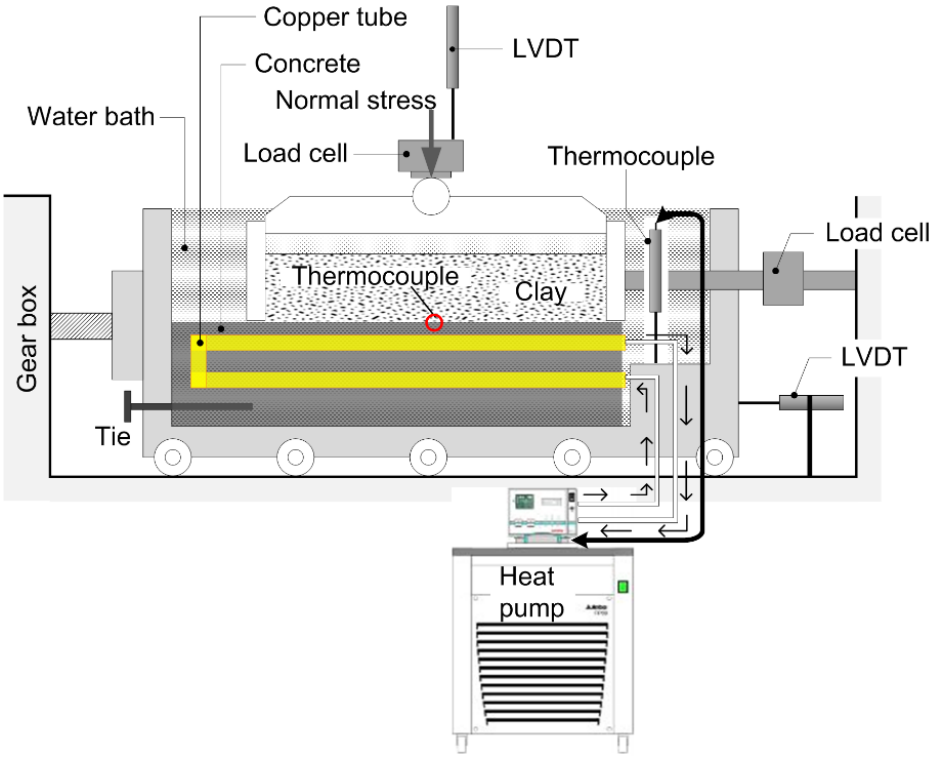

Figure 3-6: Schematic of clay–concrete direct shear test

A concrete plate with 152.4 mm (L) × 152.4 mm (W) × 25.4 mm (H) was positioned directly below the Kaolin specimen. The left end of the concrete plate was tied to the outer shear box to prevent the relative movement of the plate's left end during the shearing phase. The heat carrier fluids ran through a flexible copper tube embedded inside the concrete plate to control its temperature. Two K-type thermocouples, one at the soil-concrete interface and one inside the water bath to control the heat pump, were used to

control the heat pump.

3.3 Slow Direct Shear Test

The modified direct shear test set for clay, as shown in Figure 3-7, consists of a conventional direct shear apparatus, a plastic tube to heat/cool the water bath around the soil specimen, two K-type thermocouples, and a thermo-controller unit with the accuracy of ±0.01°C. The inner dimensions of the specimen box were 101.6 mm (L), 101.6 mm (W), and 36.5 mm (H).

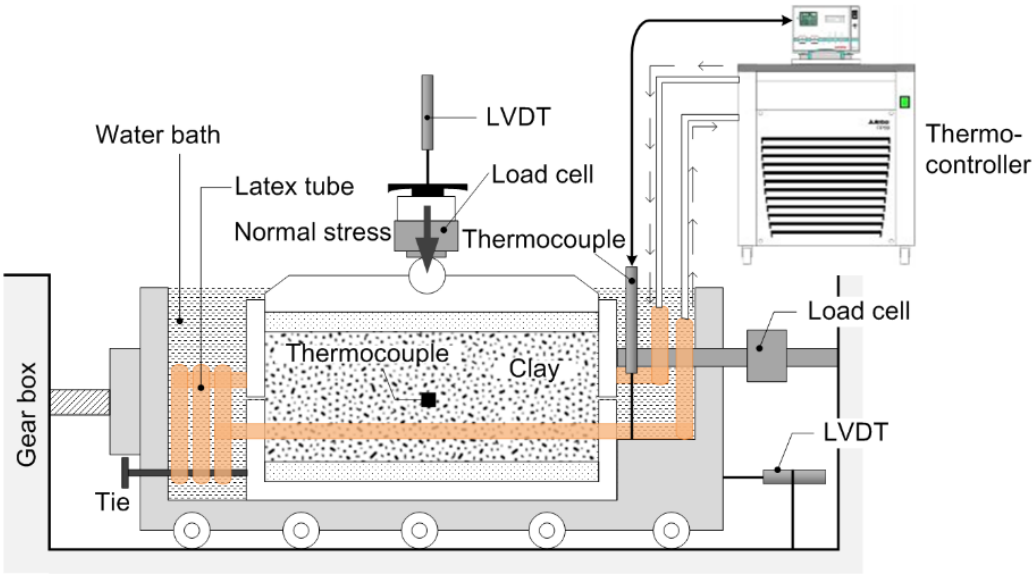

Figure 3-7: Schematic of modified direct shear test apparatus for clay

The temperature of the sample is indirectly increased/decreased by heating/cooling the water in the space between the outer box and the specimen box. There are two K-

type thermocouples, one is in the sample for temperature measurements and the other in the annulus space for navigating with the thermo-controller unit.

The thermal deformation of the specimen shear box due to the non-isothermal test conditions has to be taken into account, but the deformation at the temperature levels from 0°C to 25°C is too small to be measured. Hence, this study adopts the equivalent thermal expansion coefficient α_e = 1.637E-5℃$^{-1}$ of stainless steel AISI 316 measured by Abuel-Naga et al.[12] and the thermally induced equivalent vertical deformation based on a constant volume assumption change as follows:

$$\frac{\Delta H(\Delta T)}{H_0} = -\left[\frac{\Delta W(\Delta T)}{W_0} + \frac{\Delta L(\Delta T)}{L_0}\right] = -2\alpha_e T \qquad 3\text{-}1$$

where $\Delta H(\Delta T)$ = vertical deformation of the soil specimen due to the change in the specimen box width $\Delta W(\Delta T)$ and length $\Delta L(\Delta T)$ at temperature change ΔT; and H_0, W_0, and L_0 respectively represent height of the soil specimen and inner width and length of specimen box at room temperature (W_0 = L_0 = 101.6 mm).

3.4 Consolidated Drained Triaxial Test

The modified triaxial apparatus with the temperature control pump is shown in Figure 3-8. The GDS environmental triaxial automated system features the experimental stability

from -30°C to +60°C and pressures up to 4 MPa for which ranges are covering the investigating temperature gradients and stress values. The soil specimens in the test were cylinders with a diameter (D) of 50 mm, and a height (H) of 100 mm encased in a rubber membrane. The initial physical properties of the soil samples are listed in Table 2-1.

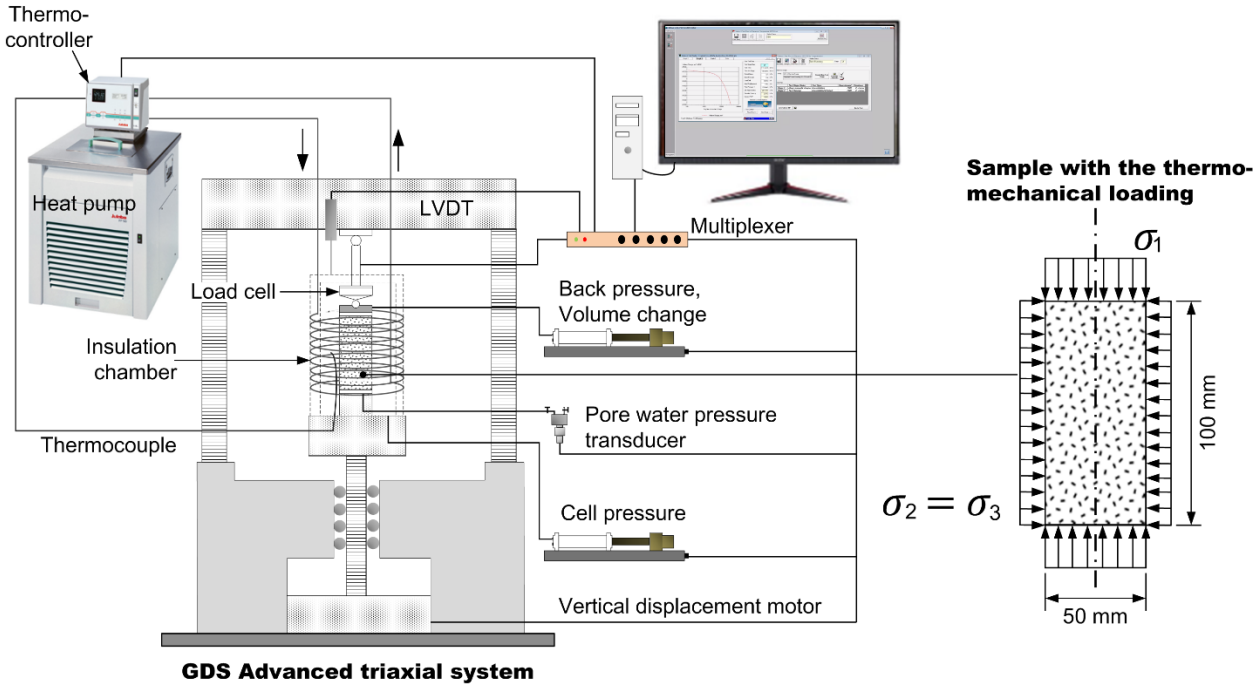

Figure 3-8: Modified triaxial apparatus with temperature controlled unit

The chamber was filled with water. Water pressure (confining pressure) was controlled by a pressure/volume controller. The other pressure/volume controller was for

controlling soil's backpressure. A K-type thermocouple connected to the heat pump was positioned at the middle height of a soil specimen. The water temperature controlled by the heat pump also simultaneously affects the soil temperature. A data acquisition system is used to collected experiment data automatically.

Chapter 4

Experiment Programs and Procedures

4 Experimental Program and Procedures

4.1 Small-Scale Pile Test

Small-scale pile tests were used herein to study the changes in the side resistance of an energy pile under extreme operating conditions. The applied thermal loadings include acyclic cooling, 36 heating/cooling cycles, and reference temperature (no temperature change). Each test began with the consolidation of the clay slurry around the pile. The following is a detailed procedure adopted in all tests.

4.1.1 Soil Preparation

Before soil placement, the pile was positioned in the middle of the chamber through a predrilled circular opening at the bottom of the compression chamber. A vertical constraint was then placed at the bottom of the pile to hold it in place during soil consolidation (Figure 4-1).

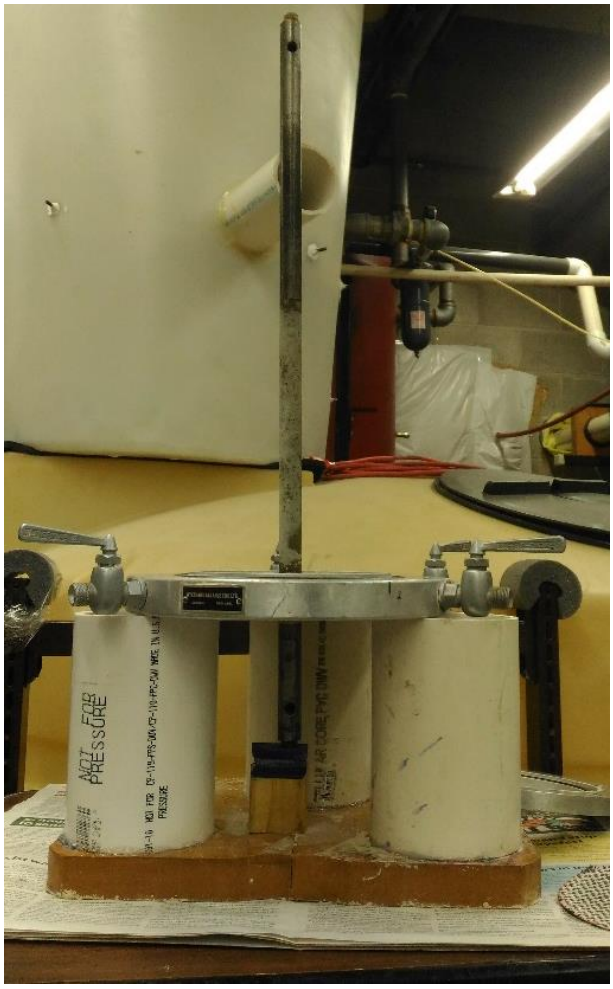

Figure 4-1: Model pile and the bottom constraint

Three K-type thermocouples and one Pore Water Pressure (PWP) probe were positioned 101.6 mm from the base. Thermocouples were attached to an 18-gauge wire to hold them in position during consolidation stage. The steel shaft was lubricated at its two extremities, so it can be assumed that the friction was only from the concrete shaft

interaction with the soil.

After positioning the model pile, the chamber is filled with Kaolin slurry and incremental vertical pressure is applied at the top of soil. A dead weight was initially applied to the slurry as a sitting consolidation pressure of 10 kPa. A doughnut-shaped airbag was then used to continue the process until a pressure of 100 kPa was reached (Figure 4-2).

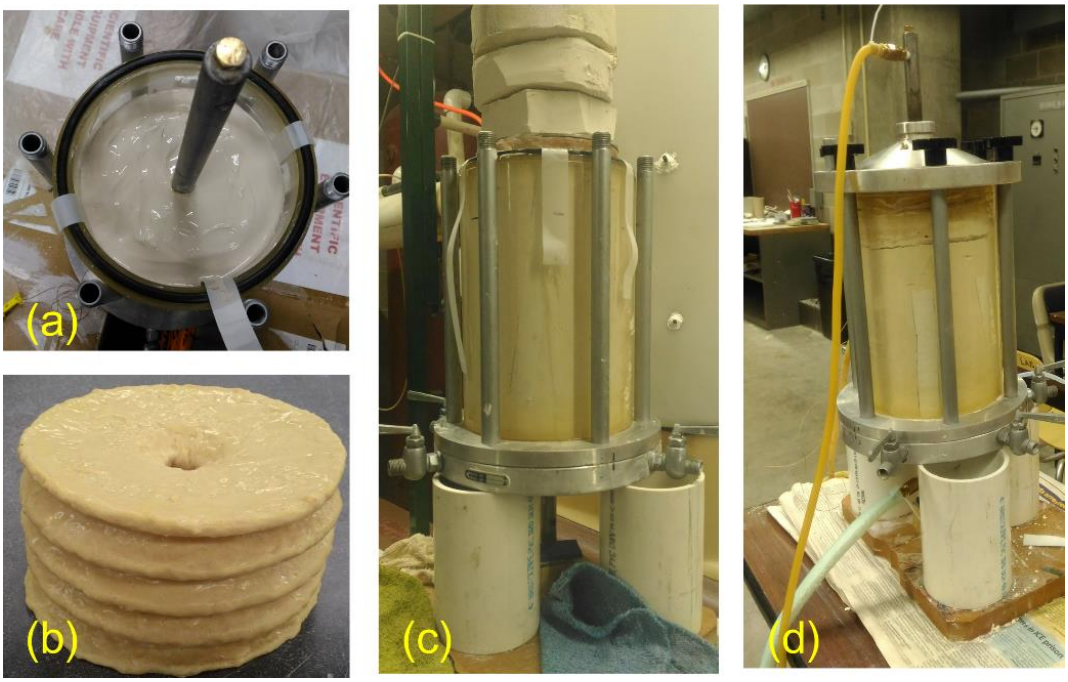

Figure 4-2: Specimen preparation for small-scale pile test

Each pressure increment was maintained until the consolidation settlement rate under

the applied pressure was insignificant. During consolidation, drainage took place vertically through the base plate and through a series of evenly spaced filter strips placed vertically on the inner wall of the chamber to facilitate radial consolidation (Figure 3-5).

4.1.2 Thermal Load Application

Upon completion of consolidation under 100 kPa, the height of the soil column was about 203.2 mm. At the same time, the PWP measuring device was fully saturated due to the water drained through the porous stone during consolidation stage (Figure 4-3).

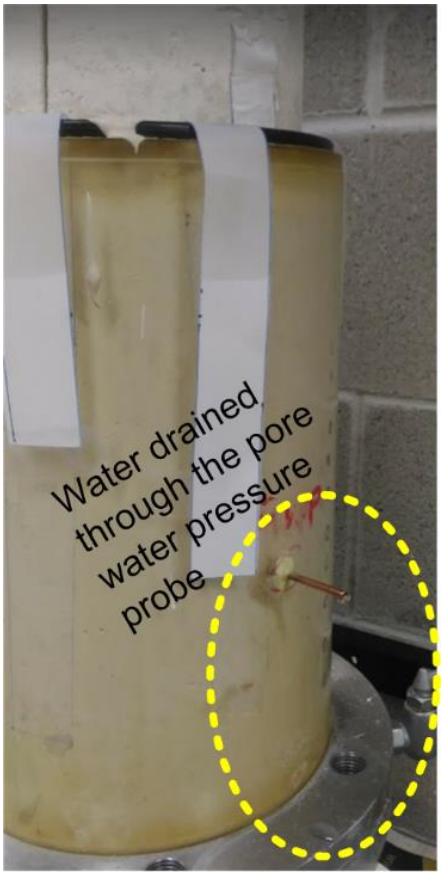

Figure 4-3: Water drained through the PWP probe during the consolidation stage

Following the consolidation stage, the pile was connected with the heat pump for heat cycle application. Circulation of the heat carrier fluid in a pile is from top to bottom, as shown in Figure 3-1(a). The chamber was thermally isolated by foam wrap materials to reduce heat exchange with ambient air, and its water outlets were closed so that the PWP transducer can monitor the thermally induced pore water pressure. To improve the

efficiency of the test, 18°C was chosen as the natural temperature of soil, which is close to the ground temperature (15°C).

A thermal cyclic loading is used to cool the soil near the pile surface from 25°C to 18°C by cooling the fluid from 25°C to 8°C in 5 minutes and holding it at the current temperature of 8° for 410 minutes. That is followed by a heating/cooling cycle (-5°C ↹ 20°C) consisting of refrigerating the fluid from its present temperature to -5°C in 5 minutes and holding it at -5°C for 240 minutes, then heating the fluid in 5 minutes to 20°C and keeping it at 20°C for 240 minutes. One heating/cooling cycle causes the soil temperature in the vicinity of the pile drop to about13.4°C and return to about 18.2°C, thus making the operational fluctuation of soil temperature, ΔT, less than 5°C within a given cycle as shown in Figure 4-4.

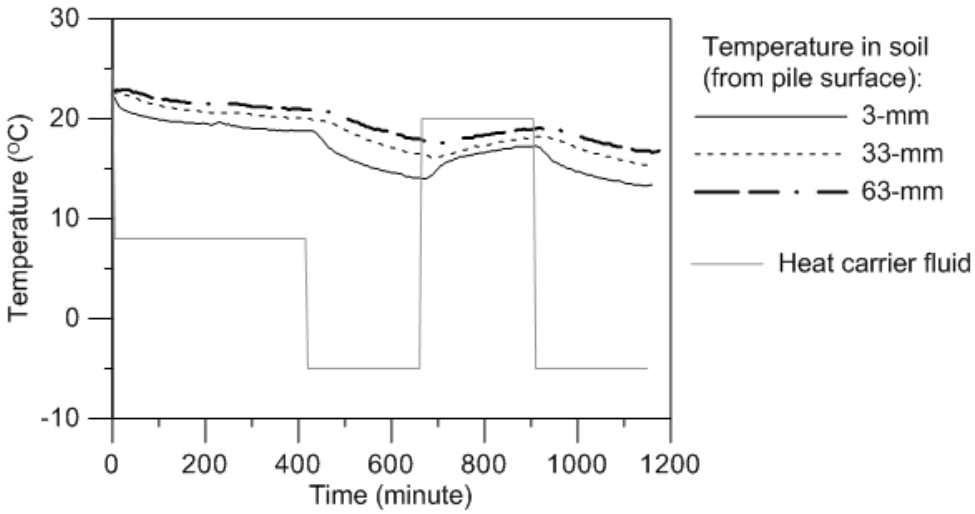

Figure 4-4: Variation of heat carrier fluid and soil temperature

4.1.3 Static Load Application

At the end of consolidation, the constraint at the bottom of the pile is removed so that when an axial load is applied to the pile, the pile can move freely in the axial direction (see Figure 3-1(b)). The loading procedure adopted “Quick Test Procedure” in ASTM D1143/ D1143M-07e1, which loads the pile in increments of 5% of the expected failure load and records the pile’s axial movement.

Deep foundations, as shown in Figure 4-5, transfer applied axial load to the ground through side friction and end bearing, but the tested pile has no end support and therefore the entire applied load transfers to the surrounding soil through side friction.

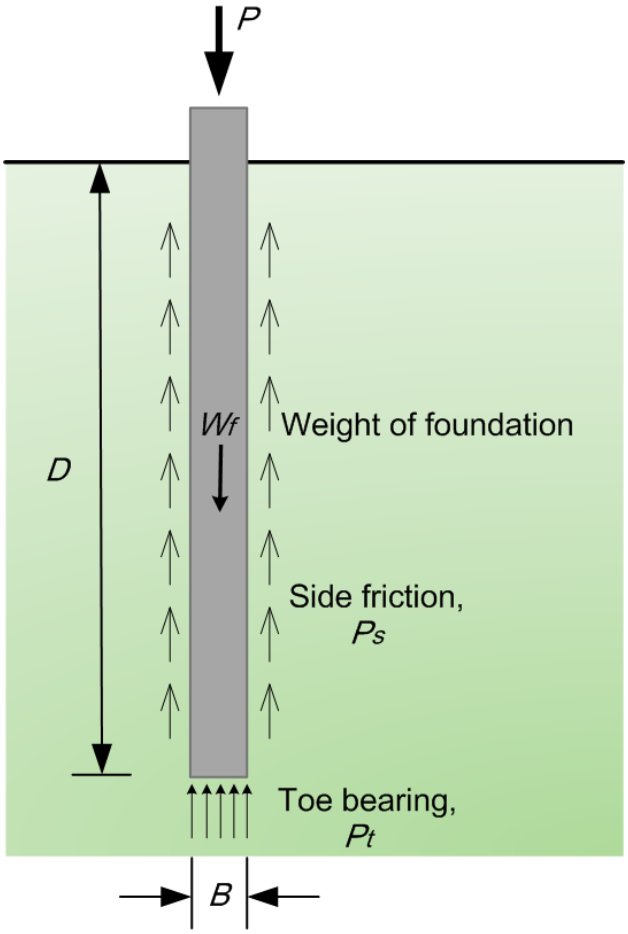

Figure 4-5: Transfer of axial loads from a deep foundation into ground by side friction and toe bearing [25]

The allowable compressive load capacity, P_a, and load increase on pile can be computed as follow equations:

$$P_a = \frac{P_{ult}}{F} = \frac{P_s - W_f}{F} = \frac{\sum f_s A_s - W_f}{F} \quad 4\text{-}1$$

where

P_a = allowable compressive load capacity

P_{ult} = ultimate compressive load capacity

P_s = side-friction resistance

W_f = weight of foundation (here is 2.3 N)

f_s = unit side-friction resistance

A_s = side-friction contact area (here is 14,187 mm^2)

F = factor of safety, ranges from 2.0 to 3.5 for compressive loading [26]

Unit side-friction resistance can be estimated through the beta method [27]:

$$f_s = \beta \sigma_z' \qquad 4\text{-}2$$

where

β = Bjerrum-Burland coefficient

σ_z' = effective overburden stress

According to Equation (4-2), the calculated unit side friction of the pile is 0.015 N/mm^2. In this equation an effective overburden pressure is the same as the one applied in all pile tests (=100 kPa). The Bjerrum-Burland coefficient is assumed to be 0.15 (see Table 4-1), and the safety factor is assumed to be 3.5.

The gross load capacity of the pile is 210 N, and the allowable compressive capacity of the pile is 60 N. The loading-control method is employed in the static loading. The load increase is 3 N/step as applying the test load in increments of 5% of the anticipated failure load. Herein the expected failure load is 60 N (the allowable compressive capacity of the pile) because the model-scale pile specimens may undergo unavoidable disturbance (unloading/positioning/reloading) in the transportation to the Instron testing machine.

The duration of each loading step is 2 hours. In each loading step, the ultimate movement of the pile will be used for the load-settlement plot in 5.1.3.

Table 4-1: Approximate range of Beta-coefficients [28]

Soil type	Friction angle (°)	Beta, β
Clay	25 – 30	0.15 – 0.35
Silt	28 – 34	0.25 – 0.50
Sand	32 – 40	0.30 – 0.90
Gravel	35 – 45	0.35 – 0.80

4.2 Slow Soil-Concrete Direct Shear Test

Slow direct shear tests were used to obtain the effective coefficient of friction between clay and foundation material after being subjected to different thermal loads. Four sets, each set comprising three samples, were used to evaluate the change in interfacial

resistance. The specimens of each group were consolidated under different stress levels (100, 150, 200 kPa). Four groups were subjected to different thermal loads that include acyclic cooling (25°C → 15°C), ten heating/cooling cycles (15°C → 5°C → 15°C), thirty-six heating/cooling cycles (15°C → 5°C → 15°C), and reference temperature (no temperature change).

All direct shear tests are summarized in Table 4-2. KC stands for Kaolin-concrete direct shear test, with numerical order from 1 to 3 representing normal stresses of 100, 150, and 200 kPa, respectively. TS stands for acyclic cooling (25°C to 15°C); TC1 stands for ten heating/cooling cycles; TC2 stands for thirty-six heating/cooling cycles; and TR stands for no temperature variation. The following quantities are included for each test: normal stress, σ_n; number of the heating/cooling cycles, N; time elapsed between the end of primary consolidation of the last applied consolidation pressure and the start of the shear test, t; moisture content of the soil after shear test, ω_f. The following is the procedure used in all tests.

Table 4-2: Summary of soil-concrete direct shear tests

Test No.	σ_n (kPa)	Final temperature (°C)	t (min)	Sequence of T (°C)	N	ω_f (%)
KC1-TS	100	15	100	25→15	0	29.82
KC2-TS	150	15	100	25→15	0	28.64
KC3-TS	200	15	100	25→15	0	28.12
KC1-TC1	100	15	2100	25→ 15→ (5 –15)^N	10	29.89
KC2-TC1	150	15	2100	25→ 15→ (5 –15)^N	10	26.28
KC3-TC1	200	15	2100	25→ 15→ (5 –15)^N	10	23.51
KC1-TC2	100	15	7300	25→ 15→ (5 –15)^N	36	29.53
KC2-TC2	150	15	7300	25→ 15→ (5 –15)^N	36	–
KC3-TC2	200	15	7300	25→ 15→ (5 –15)^N	36	–
KC1-TR	100	25	–	25	–	29.94
KC2-TR	150	25	–	25	–	29.12
KC3-TR	200	25	–	25	–	27.58

Note: σ_n, normal stress; t, elapsed time between the end of primary consolidation of the last mechanical load applied and the start of the shear test; N, number of thermal cycles; ω_f, moisture content of the clay after shear test.

4.2.1 Soil Preparation

All samples were prepared in the specimen box of the direct shear apparatus. The inner dimensions of the specimen box are 101.6 mm (L), 101.6 mm (W), and 36.5 mm (H), and the lower half of the box was lubricated. The box is filled with the Kaolin slurry having a water content of 70% and incrementally subjected to normal stress to consolidate the soil until the effective consolidation pressure is reached 100 kPa. After that, the normal stress is brought to zero and the lower half of the box is removed. The

soil in the upper half is then trimmed to a thickness of 19.4 mm (H) (Figure 4-6).

Figure 4-6: Kaolin specimen trimming (for slow soil-concrete direct shear test)

4.2.2 Sample Assembly

As shown in Figure 3-6, the concrete plate was positioned directly below the Kaolin specimen. The left end of the concrete plate was tied to the outer shear box to prevent the relative movement of the plate's left end during heating/cooling cycles and during shearing. There are two K-type thermocouples, one at the soil-concrete interface for temperature measurements and the other in the water bath for controlling the heat pump.

The normal stress is then applied gradually to specimen until the effective stress of clay reached the test level (100, 150, or 200 kPa)

4.2.3 Thermal Load Application

Drained cooling/heating cycle were applied (10 and 36 times) to the soil-concrete specimen to simulate weekly and monthly operations of a geothermal pile. Changing soil temperature under drained conditions is referred to as the drained thermal load, which implies that there is no excess pore pressure caused by temperature variation. The drained thermal load is realizable by using one of two available methods. The first method involves a slow heating/cooling rate under a zero pore pressure condition controlled by artificial intelligence [29]. The second approach involves raising the temperature incrementally until the volume change at the current temperature is steady [12]. Because the direct shear device does not have any pore water pressure measurement, the second method has been used in the tests.

According to preliminary tests, the soil specimen can achieve drained condition if it is heated/cooled at a rate of 0.2°C/min and then placed at the current temperature for 50 minutes. All in all, the rate of heating/cooling a specimen is 5°C/hour. It took 2000 and

7200 minutes to repeat the temperature cycle ten times and thirty-six times, respectively, and it took 100 minutes to cool the specimen from 25°C to 15°C.

4.2.4 Shear Displacement Application

The specimens subjected to acyclic cooling and heating/cooling cycles were sheared at 15°C, while those with no temperature variation were sheared at 25°C. Shear tests were carried out with a displacement rate of 0.003 mm/min that is small enough to avoid the effect of shear rate on the soil behavior. The maximum shear displacement at which shearing stops is set to 10 mm. This value is 10% of the soil specimen width in the shearing direction. The contact area between soil and concrete remains constant during shear because the concrete plate is larger than clay specimen.

4.3 Slow Direct Shear Test

The direct shear apparatus has been used to study the creep of NC clay after being subjected to different cyclic thermal loads. Three sets, each set comprising three specimens, were used to measure thermal creep. The specimens of each set were consolidated under different stress levels (100, 150, 200 kPa), and were subjected to acyclic cooling (25°C to 15°C) and drained cooling/heating cycles (15°C → 5°C → 15°C).

10 and 36 drained cooling/heating cycles were applied to simulate weekly and monthly operations, respectively, for a geothermal pile.

The consolidation step takes about 1 day and the thirty-six heating/cooling cycles take about 5 days. This duration of temperature variation becomes a factor affecting soil thermo-mechanical behavior as the state of a geotechnical material changes as a function of the time, i.e., aging [14].

In order to study the influence of aging on the thermo-mechanical behavior of Kaolin clay at different stress levels, two experimental sets, each set comprising three specimens, have been used. The specimens of each group have been consolidated under different vertical effective pressures (100, 150, 200 kPa) and aged for a pre-determined duration (0 – 7300 minutes).

Figure 4-7 shows the paths followed in three-dimensional space (Aging time-shear stress-temperature). Generally, the procedure for carrying out the direct shear tests was as follows:

i. Complete preliminary consolidation under different stress levels at 25°C (point 0)

ii. Drained cooling (path 0 → 1)

iii. Drained cooling (path 1 → 2)

iv. Drained heating (path 2 → 1)

v. Repeat sequences (iii) to (iv) 10 and 36 times

vi. Specimens which skipped steps (ii) through (v) but aged 7300 minutes at 25°C (path 0 → 3) are for investigating the time-dependent behavior

vii. Drained shearing (path 0 → 4 or 3 → 4 for tests at 25°C; path 1 → 4 for tests at 15°C), by applying shear displacement at a rate of 0.003 mm/min.

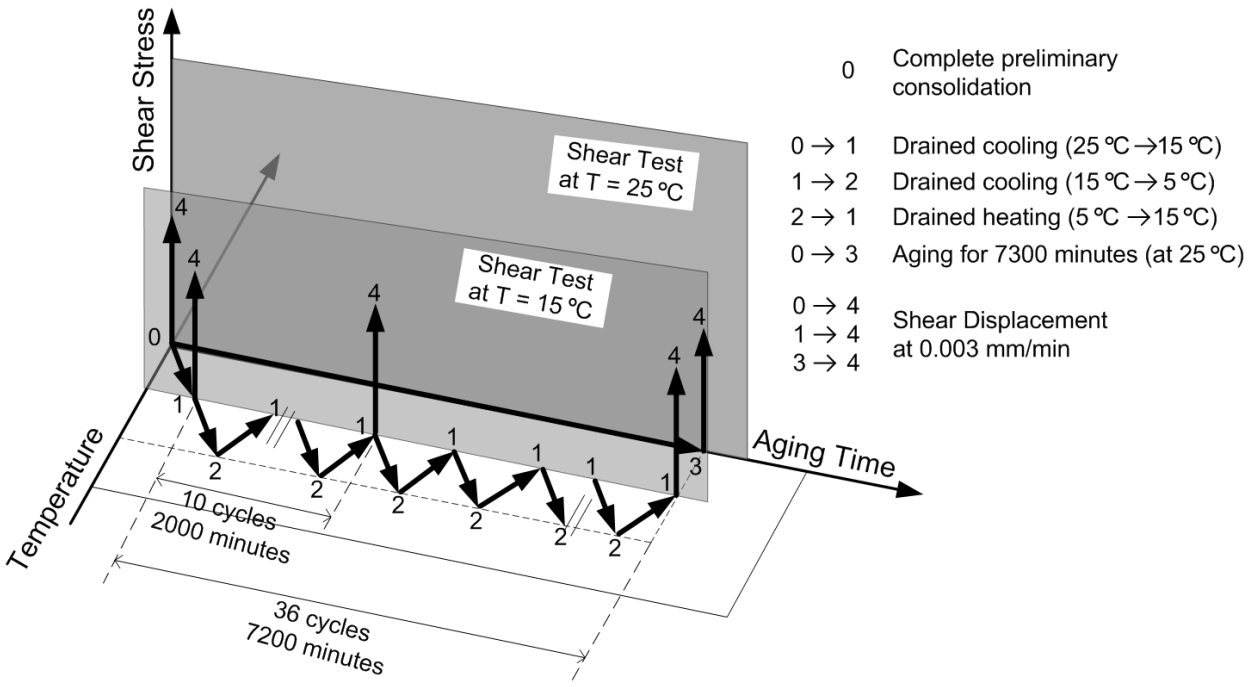

Figure 4-7: Thermo-mechanical testing paths

All direct shear tests on Kaolin are summarized in Table 4-3. KK stands for direct shear test on Kaolin clay, with numerical order from 1 to 3 representing normal stresses of 100, 150, and 200 kPa performed on specimens, respectively. TS stands for acyclic cooling (25°C to 15°C); TC1 stands for ten heating/cooling cycles; TC2 stands for thirty-six heating/cooling cycles; TR1 stands for no temperature variation nor ageing; and TR2 stands for no temperature variation but aged for 7300 minutes. The following quantities are included for each test: normal stress, σ_n; number of the heating/cooling cycles, N; time elapsed between the end of primary consolidation of the last applied consolidation pressure and the start of the shear test, t; moisture content of the soil after shear test, ω_f. The following is the procedure used in all tests.

Table 4-3: Summary of direct shear tests on Kaolin clay

Test No.	$\boldsymbol{\sigma_n}$ (kPa)	Final temperature (°C)	t (min)	Sequence of T (°C)	N	ω_f (%)
KK1-TS	100	15	100	25→15	0	29.90
KK2-TS	150	15	100	25→15	0	29.78
KK3-TS	200	15	100	25→15	0	28.70
KK1-TC1	100	15	2100	25→ 15→ $(5-15)^N$	10	–
KK2-TC1	150	15	2100	25→ 15→ $(5-15)^N$	10	–
KK3-TC1	200	15	2100	25→ 15→ $(5-15)^N$	10	–
KK1-TC2	100	15	7300	25→ 15→ $(5-15)^N$	36	31.08
KK2-TC2	150	15	7300	25→ 15→ $(5-15)^N$	36	29.19

Test No.	σ_n (kPa)	Final temperature (°C)	t (min)	Sequence of T (°C)	N	ω_f (%)
KK3-TC2	200	15	7300	25→ 15→ (5 –15)^N	36	–
KK1-TR1	100	25	–	25	–	30.70
KK2-TR1	150	25	–	25	–	29.30
KK3-TR1	200	25	–	25	–	29.07
KK1-TR2	100	25	7300	25	–	30.55
KK2-TR2	150	25	7300	25	–	29.30
KK3-TR2	200	25	7300	25	–	28.68

Note: σ_n, normal stress; t, elapsed time between the end of primary consolidation of the last mechanical load applied and the start of the shear test; N, number of thermal cycles; ω_f, moisture content of the clay after shear test.

4.3.1 Soil Preparation

All samples were prepared in the specimen box of the direct shear apparatus. The inner dimensions of the specimen box are 101.6 mm (L), 101.6 mm (W), and 36.5 mm (H). The box with Kaolin slurry having a water content of 70% and an increment normal stress is applied to consolidate the soil until the effective consolidation pressure of 100 kPa is reached. The normal stress is removed, and then gradually increased to the specified stress level (100, 150, 200 kPa)

4.3.2 Thermal Load Application

Thermal load application is the same as in section 4.2.3.

4.3.3 Shear Displacement Application

The specimens subjected to the acyclic cooling and heating/cooling cycles were sheared at 15°C, while those with no temperature variation were shear at 25°C. Shear tests were carried out with a displacement rate of 0.003 mm/min that is small enough to avoid the effect of shear rate on the soil behavior. The maximum shear displacement at which shearing stops is set to 10 mm.

4.4 Consolidated Drained Triaxial Test

Triaxial tests have been used to study the thermo-mechanical behavior of over-consolidated (OC) clay and NC clay and the effect of aging on NC clay that is subjected to cyclic thermal load. For OC clay, three sets, each set comprising one specimen, were used to investigate the effect of cyclic thermal load on soil stiffness and peak and ultimate shear strength. For NC clay, five groups (at least one specimen per group) were used to study the thermal creep and assess the thermo-mechanical behaviors of soil.

The effective confining pressure on OC clay was 50 kPa and the pre-consolidation pressure was 100 kPa. The effective confining pressures on NC clay samples were 150 and 200 kPa. Except for samples at constant temperature (constant 25°C), each set of

samples was subjected to acyclic cooling (25°C to 15°C) and drained cooling/heating cycles (15°C → 5°C → 15°C). The drained cooling/heating cycle was repeated 36 times to simulate monthly operations for a geothermal pile.

All triaxial tests on Kaolin are summarized in Table 4-4. K stands for triaxial test on Kaolin clay, with numerical order from 1 to 3 representing effective confining pressures of 50, 150, and 200 kPa, respectively. TS stands for acyclic cooling (25°C to 15°C); TC stands for thirty-six heating/cooling cycles; TR stands for no temperature variation nor ageing; and TR2 stands for no temperature variation but aged for 16 days.

The following quantities are included for each test: normal stress, σ_n; number of the heating/cooling cycles, N; time elapsed between the end of primary consolidation of the last applied consolidation pressure and the start of the shear test, t; moisture content of the soil after shear test, ω_f. The following is the procedure used in all tests.

Table 4-4: Summary of triaxial tests

Test No.	σ_3' (kPa)	Final temperature (°C)	t (min)	Sequence of T (°C)	N	ω_f (%)
K1-TS	50	15	300	22→15	0	31.54
K2-TS	150	15	300	22→15	0	28.75
K3-TS	200	15	300	22→15	0	27.79
K1-TC	50	15	23340	22→ 15→ $(5-15)^N$	36	31.00

Test No.	σ_3' (kPa)	Final temperature (°C)	t (min)	Sequence of T (°C)	N	ω_f (%)
K2-TC	150	15	23340	22→ 15→ (5 –15)^N	36	28.02
K3-TC	200	15	23340	22→ 15→ (5 –15)^N	36	27.15
K1-TR	50	25	–	22	–	30.80
K2-TR	150	25	–	22	–	29.40
K3-TR	200	25	–	22	–	27.41
K3-TR2	200	25	23340	22	0	27.40

Note: σ_3', effective confining pressure; t, elapsed time between the end of primary consolidation of the last mechanical load applied and the start of applying deviator stress; N, number of thermal cycles; ω_f, moisture content of the clay after test.

4.4.1 Soil Preparation

Kaolin clay specimens were produced using a consolidation mold (pipe) shown in Figure 4-8. Dimensions of the consolidation mold are 127 mm in inner diameter (ID) and 254 mm in height (H). A clay slurry having a water content of 70% is placed in the mold and a consolidation pressure of 100 kPa is applied using a dead weight. Afterward, the normal stress is removed and the soil specimen is removed and trimmed into a diameter of 50 mm and height of 100 mm.

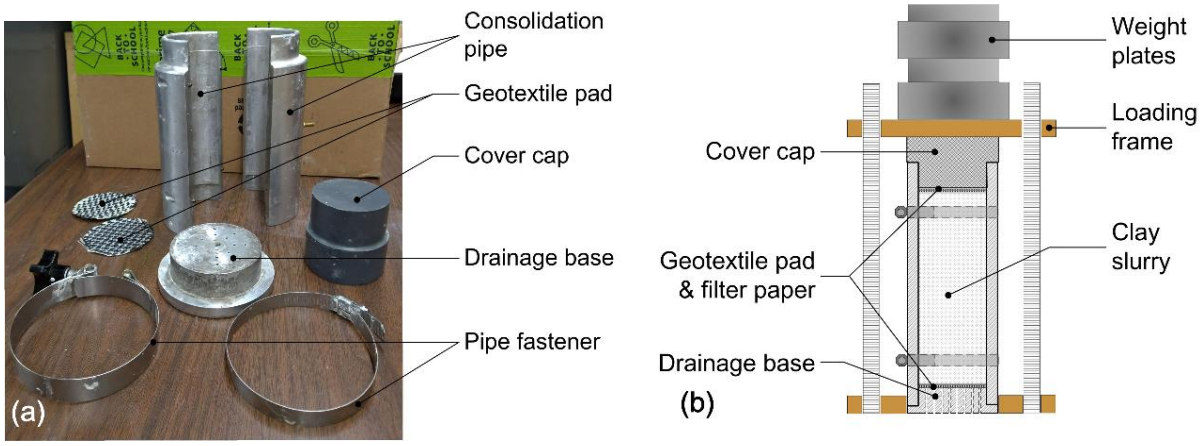

Figure 4-8: Triaxial sample preparation kit (a) mechanical components (b) schematic

Soil column was produced in a kit of consolidation pipe as shown in Figure 4-8. Dimensions of the consolidation pipe are 127 mm in inner diameter (ID) and 254 mm in height (H). The interfaces of pipe were lubricated. Filled the consolidation pipe with the Kaolin slurry having a water content of 70% and incrementally applied load to the top of soil. The weights were applied to the slurry as consolidation load until the pressure reached 100 kPa. Afterward, the normal stress and the consolidation pipe were removed and the soil was trimmed into a soil column with a diameter (D) of 50 mm and a height (H) of 100 mm (Figure 4-9).

Figure 4-9: Triaxial specimen

4.4.2 Thermal Load Application

Under drained conditions, the soil specimen is subjected to acyclic cooling or heating/cooling cycles. The drained heating/cooling cycle was repeated 36 and 100 times, respectively, to simulate monthly and seasonal operations for a geothermal pile.

The drained thermal load can be achieved by using one of the two methods mentioned in section 4.2.3. In order to maintain the consistency of the experiment, the second method was adopted in triaxial tests, that is, gradually increasing the temperature until the volume change at the current temperature is stable.

According to preliminary tests, the soil column can achieve a drained condition if it is heated/cooled at a rate of 0.05°C/min and then placed at the current temperature for 120 minutes. It took 23040 minutes (16 days) and 64000 minutes (45 days) to repeat the heating/cooling cycle thirty-six times and one hundred times, respectively, and it took 300 minutes to cool the specimen from 25°C to 15°C.

4.4.3 Axial Displacement Application

The specimens subjected to the acyclic cooling and heating/cooling cycles were sheared at 15°C, while those without temperature variation were shear at 25°C. Axial displacement was applied at a rate of 0.001 mm/min that is small enough to avoid the effect of shear rate on the soil behavior. The maximum axial displacement at which shearing stops is set to 15 mm. This value is 15% of the soil column height in the axial direction.

Chapter 5

Results and Discussions of the Results

5 Experimental Results

5.1 Small-Scale Pile Test

The isothermal pile is subjected to loads at a constant temperature of 25°C, while the acyclic cooled pile and the pile with heating/cooling cycles are subjected to axial loads at 15°C. The temperature of the latter tests us the temperature of the heat carrier fluid since the temperature of the pile and the soil in acyclic cooled pile the and the pile with heating/cooling cycles never reached a steady state as indicated in Figure 5-1.

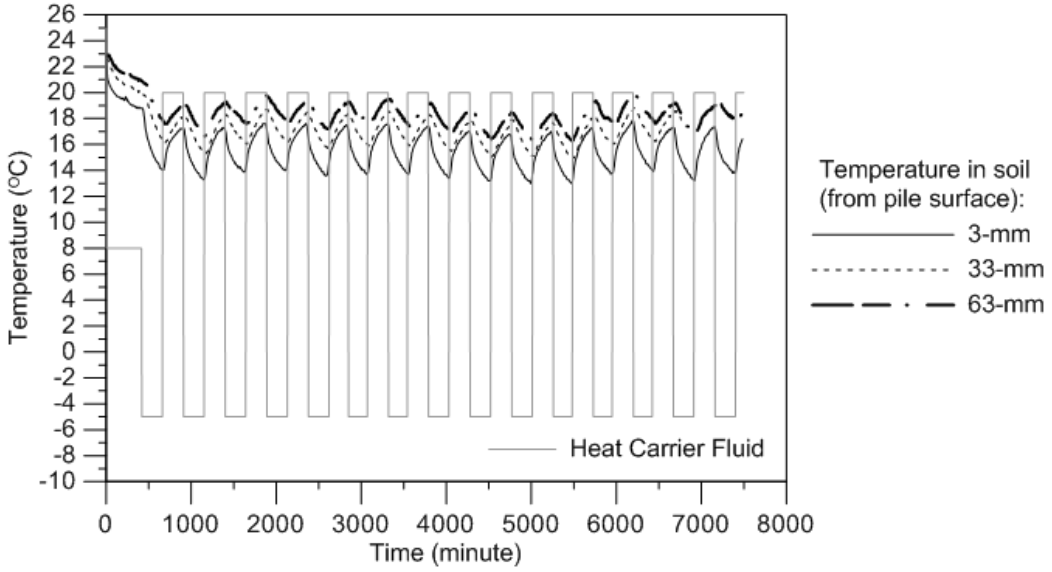

Figure 5-1: Temperature variations in clay

5.1.1 Radial Temperature Distribution

The radial temperature distribution in clay during heating/cooling cycling is shown in

Figure 5-1 (only 15 cycles are shown in the figure). At three radial distances from the pile's surface (3 mm, 33mm, 63 mm), the radial temperature fluctuation (ΔT) was 4°C, 2°C, and 1°C, respectively. The radial temperature gradient in the figure implies that the thermal boundary of an individual pile exceeds 2.8 times the pile's diameter, but whether this result represents field conditions is inconclusive.

The radius of the surrounding soil in the model was 3.4 times the pile diameter that is greater than the minimum center-to-center spacing of 3.0 diameters allowed by AASHTO (2014) [30]. Thus, the surrounding soil in the test was adequate to study the thermal influence zone of an individual pile from a practical standpoint. Nevertheless, the volume of heat carrier fluid flowing inside the pile is large relative to the pile volume in the model, so heat flux leaving the pile surface is possibly higher than the operation of a prototype energy pile. Due to the low value of heat flux along the real pile surface, the change in soil temperature around a prototype energy pile may be smaller than that in the model.

5.1.2 Thermally Induced Excess Pore Water Pressure (PWP)

The heating/cooling rate in pile tests did not meet drainage standards, plus the

drainage valves were closed in heating/cooling cycles (Figure 5-2). Under undrained conditions, thermally induced pore water pressure is likely to change with temperature if no material in/out and thermal expansion coefficients remain constant.

Figure 5-2: The water drainage valves were turned off during heating/cooling

The thermal expansion coefficient of water is approximately six times that of clay particle (γ_{clay} = 3.5E-5/℃; γ_{water} = 2.14E-4/℃). The thermal contraction of clay particles is much lower than that of water upon cooling. Theoretically, if the current temperature is

lower than the initial temperature, PWP will be lower than the initial value. Conversely, the measured value will be greater than the initial value if the current temperature is higher than the initial temperature. The radial distance between the tip of the PWP probe and the surface of pile was 3 mm. Figure 5-3 shows the change of reading in PWP during heating/cooling cycles.

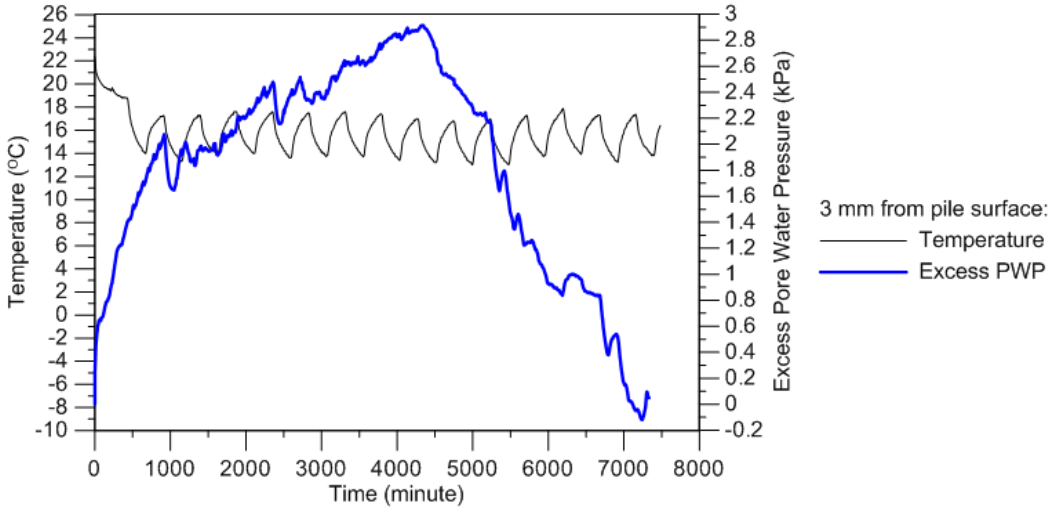

Figure 5-3: Variations of excess pore water pressure in clay

In Figure 5-3 soil temperature at distance of 3 mm from the pile dropped from 25°C to about 18°C in acyclic cooling, and the reading of the PWP transducer increased by 1.4 kPa. During subsequent cooling and heating, the reading of the PWP transducer continued to increase until it reached around 2.9 kPa. Following the 8th heating/cooling

cycle, the reading of the PWP transducer started to decrease.

Observe the PWP curve, the reading of the PWP transducer does not decrease in the cooling stage nor increase during the heating. However, in the tested temperature range, the value of PWP shall be all less than zero because (1) the temperature range of heating/cooling cycles is lower than the initial temperature (room temperature), and (2) the thermal expansion coefficient of water is approximately six times that of clay particle. This will cause the pore water pressure to decrease during the cooling process. (3) The model pile should have undergone volume contraction at a lower temperature, resulting in lateral unloading of the surrounding soil. Through observation, the influence factors on the PWP result are as follow.

The saturated clay in direct contact with the pile surface was excessively cooled and possibly frozen during the cooling stage where the temperature of the heat carrier fluid reached -5°C. Following the cooling stage, the temperature of the heat carrier fluid was increased to 18°C, thus causing the frozen clay layer to thaw. This freeze-thaw cycle caused significant contraction-expansion in the clay layer in direct contact with the pile. The contraction-expansion cycle was repeated 36 times causing the pile to lose contact

with the pile thus compromising the pile-soil interface strength.

After the 8th heating/cooling cycle, water was observed to discharge along the pile surface due to gravity and repeated radial contraction/expansion of the soil in direct contact with the pile. Also, the pile experienced radial contraction upon cooling, which caused the soil undergo a lateral unloading stress path. On the contrary, the pile experienced radial expansion upon heating, and the radial expansion induced lateral pressure on the surrounding soil. The inner diameter of soil specimen was increased under repeated lateral compressive loads. Once the increased inner diameter cannot be restored to the initial state, the space between the pile and surrounding soil is formed and became a “drainage path” for the water produced by thawing the saturated clay.

5.1.3 Load-Settlement Behavior

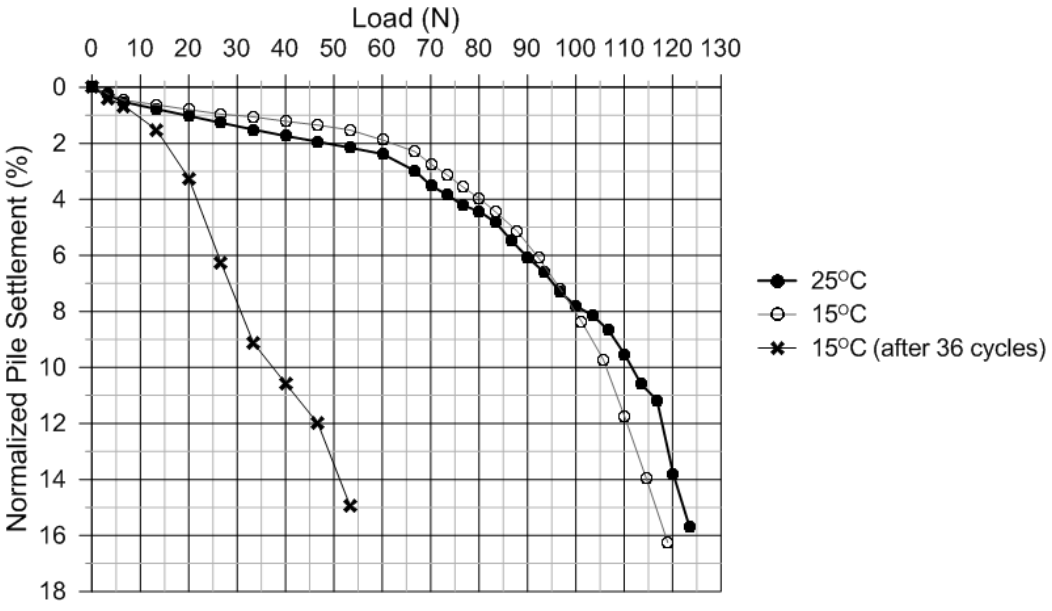

Figure 5-4: Load-settlement curves of pile head under different thermal loading paths

Figure 5-4 shows the load-settlement curves for the pile under different thermal paths. According to ASTM D1143/ D1143M – 07e1, the failure load refers to the test load at which rapid continuing, progressive movement occurs. 10% of the pile diameter is recommended on the basis that it is the minimum movement that could be associated with failure of the soil beneath the pile toe [31-33]. Whereas Hirany and Kulhawy (1989) [34] found the failure threshold generally occurs at a pile-head movement of 4% of the pile diameter.

Table 5-1 presents a summary of the test results. The failure loads of acyclic cooled pile (heat carrier fluid: 15°C) and the isothermal pile are similar, and the loads are smaller than the ultimate load capacity (180 N). However, the failure load of the pile subjected to cyclic thermal load was reduced tremendously. This sever loss of load capacity is attributed to the freeze-thaw cycles as indicated above (see Figure 5-5).

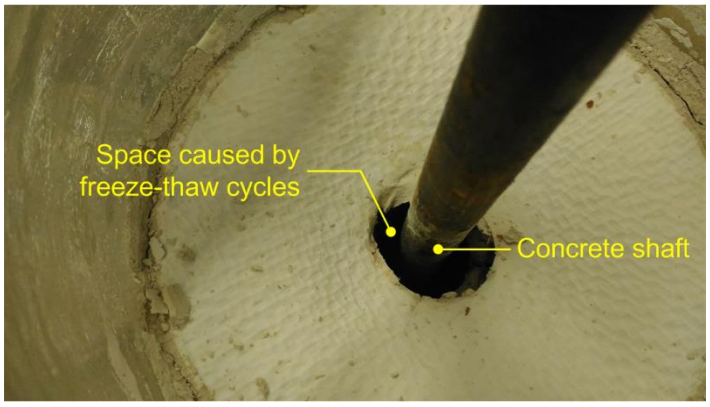

Figure 5-5: Space caused by freeze-thaw cycles

Table 5-1: Summary of small-scale pile load results

Thermal loading (heat carrier fluid temperature)	P at 4%D (N)	P at 10%D (N)	P at 15%D (N)
25°C	75	112	123
25 °C → 8°C → 15°C	80	108	117
25 °C → 8°C → -5°C ⇆ 20 °C (36 cycles) → 15°C	22	37	53

Note: P, compressive load value; D, pile diameter

5.2 Slow Soil-Concrete Direct Shear Test

5.2.1 Under Isothermal Condition

The conventional interface direct shear test is to apply the relative shear displacement on sample when soil has completed its primary consolidation at room temperature. The samples in this section did not experience temperature changes before shearing. The results are shown in Figure 5-6.

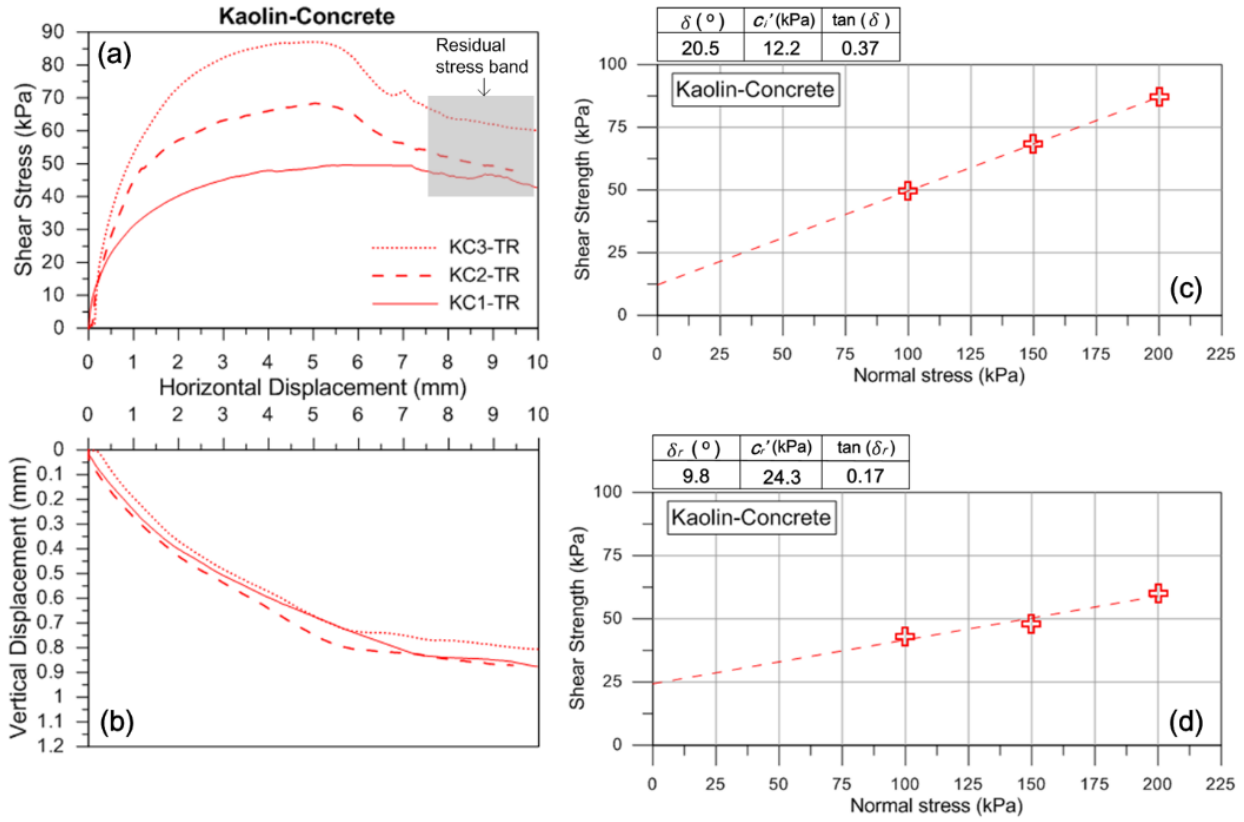

KC3-TR: normal stress was 200 kPa; no thermal load

KC2-TR: normal stress was 150 kPa; no thermal load

KC1-TR: normal stress was 100 kPa; no thermal load

Figure 5-6: Experimental results on clay-concrete interface at 25°C: (a) shear stress versus horizontal displacement; (b) vertical displacement versus horizontal displacement; (c) peak shear strength envelope; (d) residual shear strength envelope

Given the increase in normal stress, the specimen exhibited a softening behavior after the peak as shown in Figure 5-6(a). The results of vertical displacement during shearing are shown in Figure 5-6(b). During the shearing displacement, all clay

specimens exhibited contractive (non-dilative) behavior.

the clay at the three stress levels contracted from the beginning to the end. Figure 5-6(c) shows that the maximum shear strength and effective normal stress can be well correlated with a linear function (failure envelope) that is associated with the Mohr-Coulomb failure criterion:

$$\tau = c_i' + \sigma' \tan \delta \qquad 5\text{-}1$$

where

τ = shear stress

σ' = effective normal stress

c_i' = interface adhesion

δ = interface friction angle

At large shearing displacements, the residual shear strength of clay-concrete interface (τ_f) can be obtained as shown in Figure 5-6(a). Figure 5-6(d) shows the plot of τ_f versus σ'. The linear regression plot will pass through the origin and can be expressed as:

$$\tau_f = c_r + \sigma' \tan \delta_f$$

where

τ_f = residual shear stress

σ' = effective normal stress

c_r = residual interface adhesion

δ_f = residual interface friction angle

The linear correlation between peak shear strength and normal stress is determined by the result in Figure 5-6(c): the interface friction angle is 20.5° and the interface adhesion is 12.2 kPa. The residual interface friction angle is 9.8°, which can be obtained from Figure 5-6(d).

5.2.2 Thermal Effects on Shear Strength

Non-cyclically cooled specimens and cyclically cooled/heated samples were all sheared at 15°C, and the results are in Figure 5-7. It can be seen from Figure 5-7(a) that the ductility of the interface decreases with heating/cooling cycles. The curves of vertical displacement versus horizontal displacement during shearing are shown in Figure 5-7(b). The results show that the compressibility of clay is low after going through heating/cooling cycles.

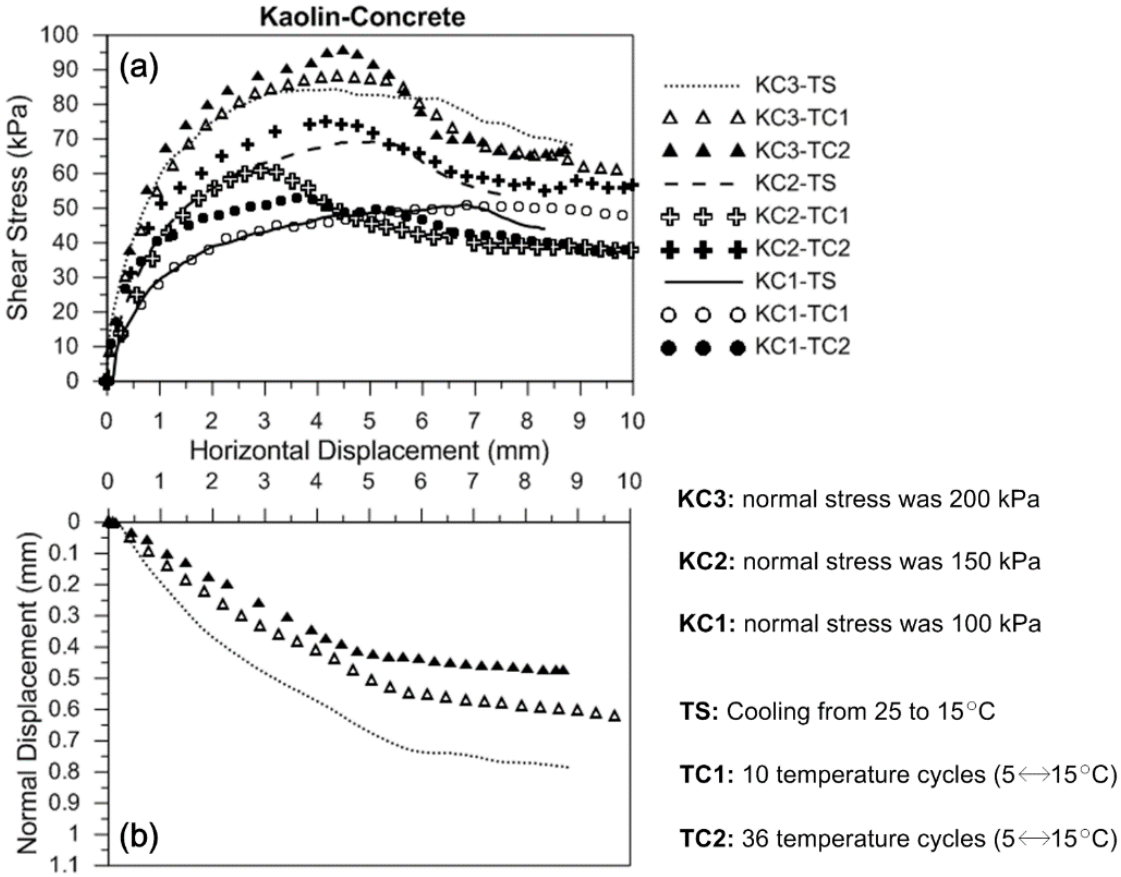

Figure 5-7: Experimental results on clay-concrete interface at 15°C: (a) shear stress versus horizontal displacement (b) vertical displacement versus horizontal displacement

Peak shear strength of clay-concrete interface is in Figure 5-8. When the number of heating/cooling cycles increased from zero to thirty-six times, the interface friction angle increases with heating/cooling cycles and the interface adhesion decreases by 43%. On the other hand, Figure 5-8(b) shows that residual friction angles are independent of the temperature paths.

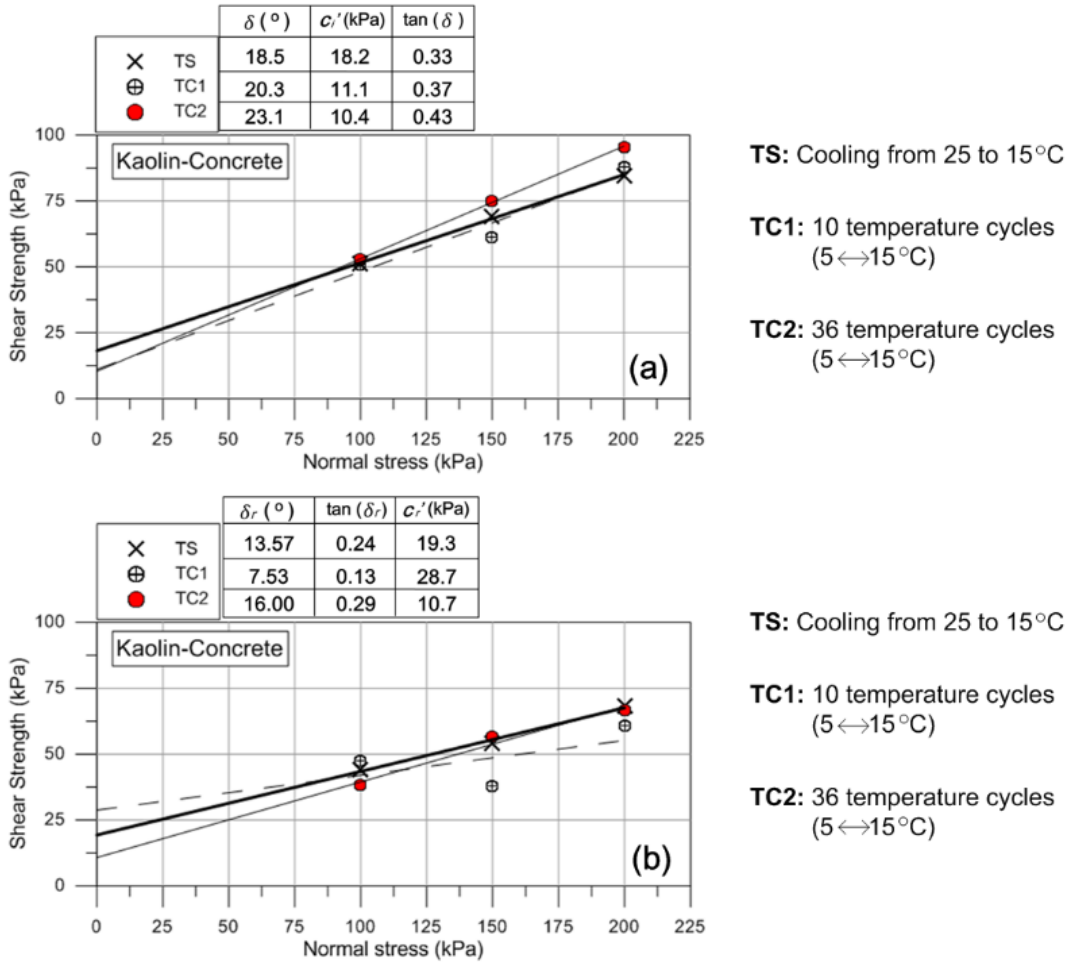

Figure 5-8: Experimental results on clay-concrete interface at 15°C: (a) peak shear strength envelope (b) residual shear strength envelope

5.3 Slow Direct Shear Test

5.3.1 Soil Creep

Figure 5-9 shows the creep of specimens subjected to 36 heating/cooling cycles and 7300 minutes of aging at two different stress levels (100 and 200 kPa). After preliminary

consolidation, one specimen (solid line) was subjected to the acyclic cooling and followed by 36 heating/cooling cycles, while the other specimen (long-dash line) was kept at a constant temperature. In drained condition, NC clay maintained at a constant temperature only showed secondary consolidation over time while under temperature cycling showed an increase in equivalent vertical compression (thermal creep). Other researchers have reached similar conclusions for different stresses, different temperature cycling ranges, and different clays [6, 7, 35, 36].

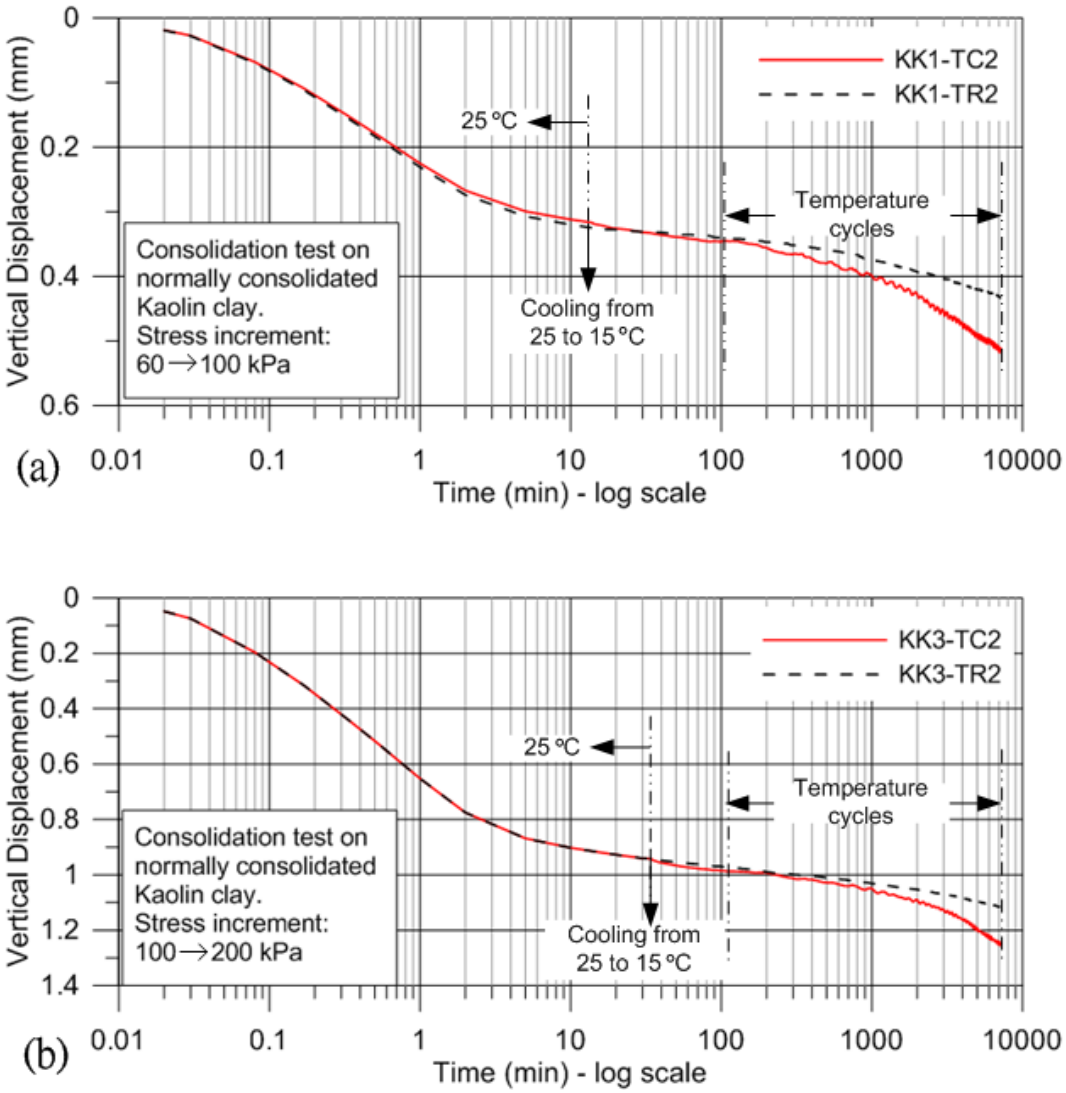

Figure 5-9: Thermal creep and aging creep under (a) 100 kPa and (b) 200 kPa

The creep with temperature variation is plotted versus time in Figure 5-10. During the heating phase (e.g. path c → d) and the initial cooling phase (path a → b), the observed compression (vertical settlement) was greater than that experienced by the specimen

held at the constant temperature. During the cooling phase in cycles (e.g. path b → c), expansion was observed, but compression occurred immediately after that. The degree of expansion at cooling is smaller than the degree of compression at heating, and thus the heat-induced creep is irreversible.

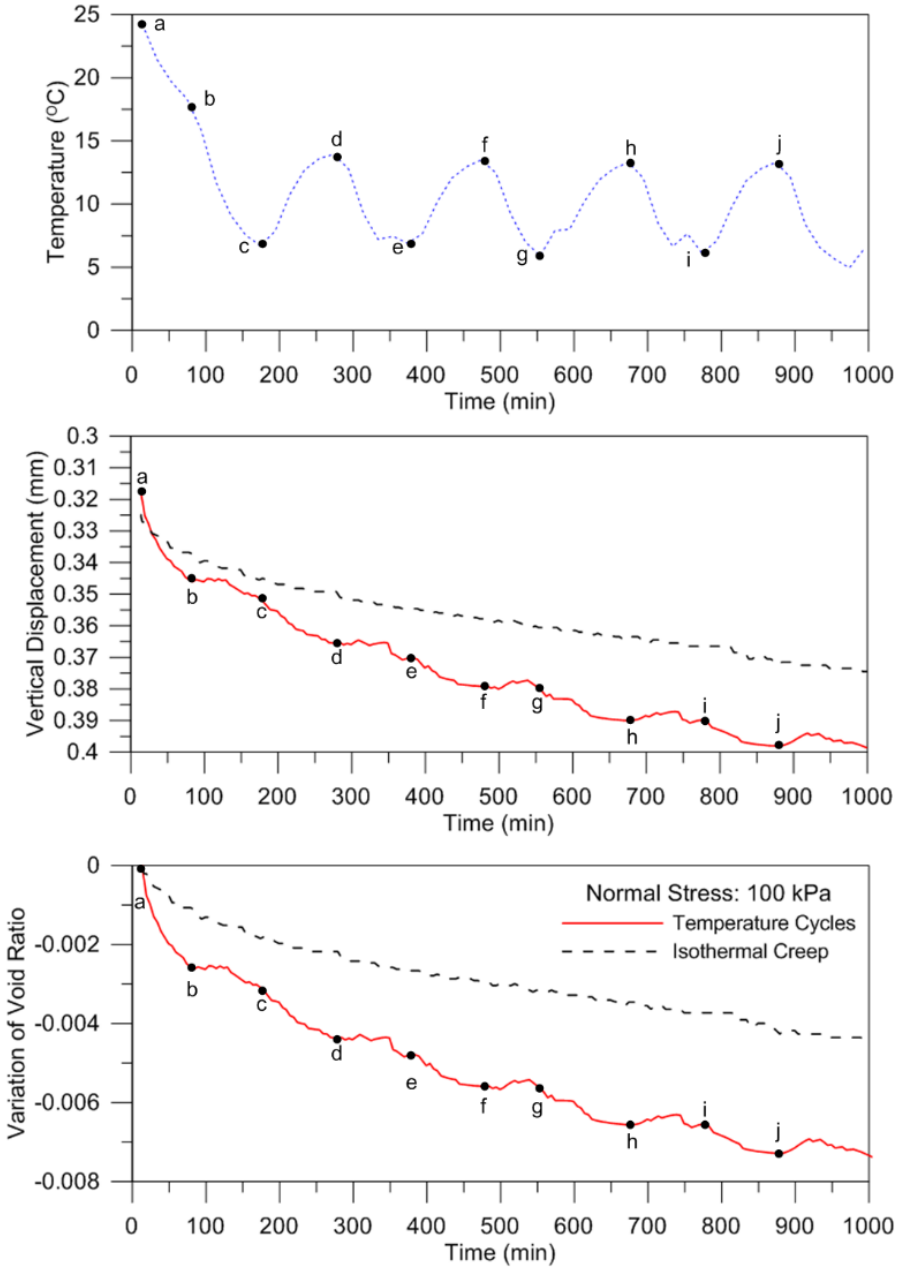

Figure 5-10: Thermal creep with temperature variation during the heating/cooling cycles

5.3.2 Thermal Effects on Shear Strength

Results on specimens sheared at 15°C are shown in Figure 5-11. At different stress levels, the shear stress increases as the number of heating/cooling cycles increases as shown in Figure 5-11(a). Results on vertical displacement versus horizontal displacement are in Figure 5-11(b), which shows that the clay contracted during shearing and shear stress/displacement curves on the acyclic and cyclic thermal loads are similar at a given pressure. Figure 5-11(c) consists of failure envelopes on the acyclic and cyclic thermal loads where c' is cohesion and ϕ' is friction angle.

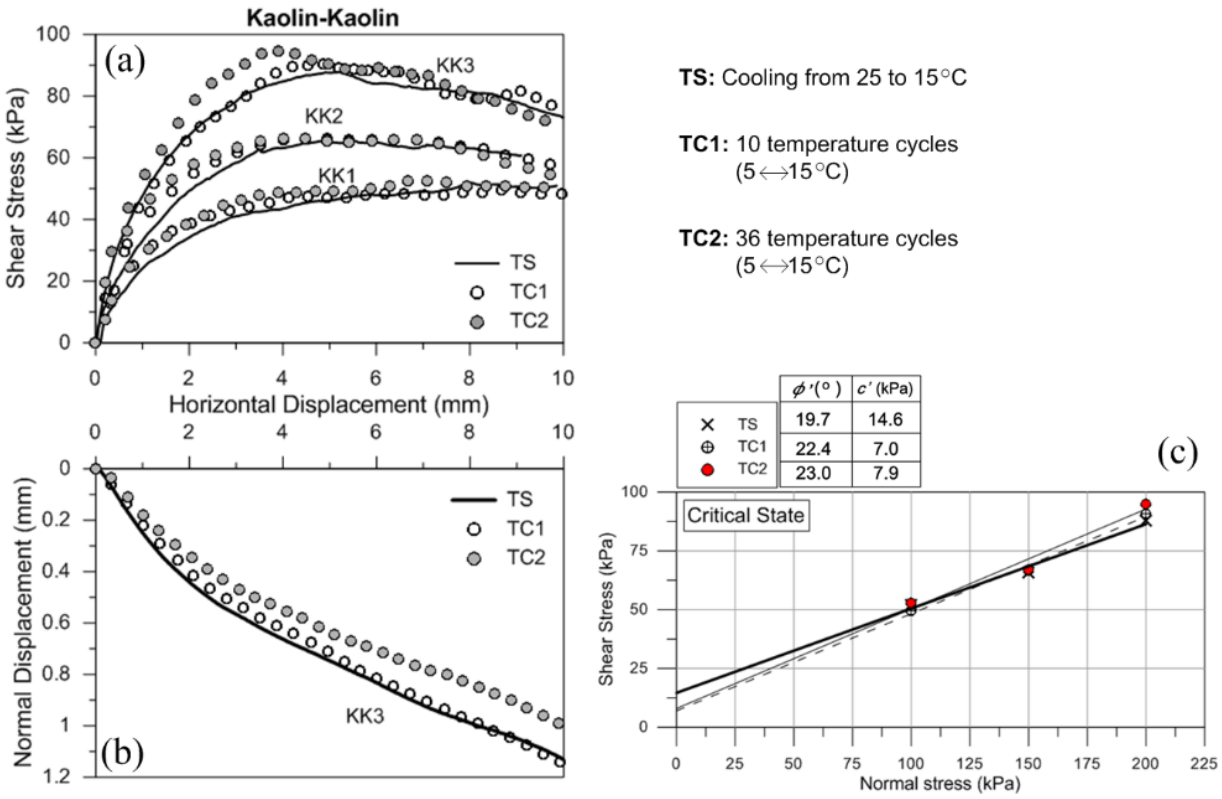

Figure 5-11: Experimental results on NC clay at 15°C: (a) shear stress versus horizontal displacement (b) vertical displacement versus horizontal displacement (c) shear strength envelope

It is observe from Figure 5-11(c), that the peak shear strength and friction angle increase as the number of heating/cooling cycles increases. Still, as the number of heating/cooling cycles increased from zero to thirty-six, the cohesion decreased by 46%.

5.3.3 Effect of Aging on Direct Shear Strength

Figure 5-12 shows results of the specimens that were subjected to two different aging times at 25°C. From Figure 5-12(c), the clay obtained more strength during increased

time in secondary consolidation, which corresponds to higher shear stress on aging (Figure 5-12(a)).

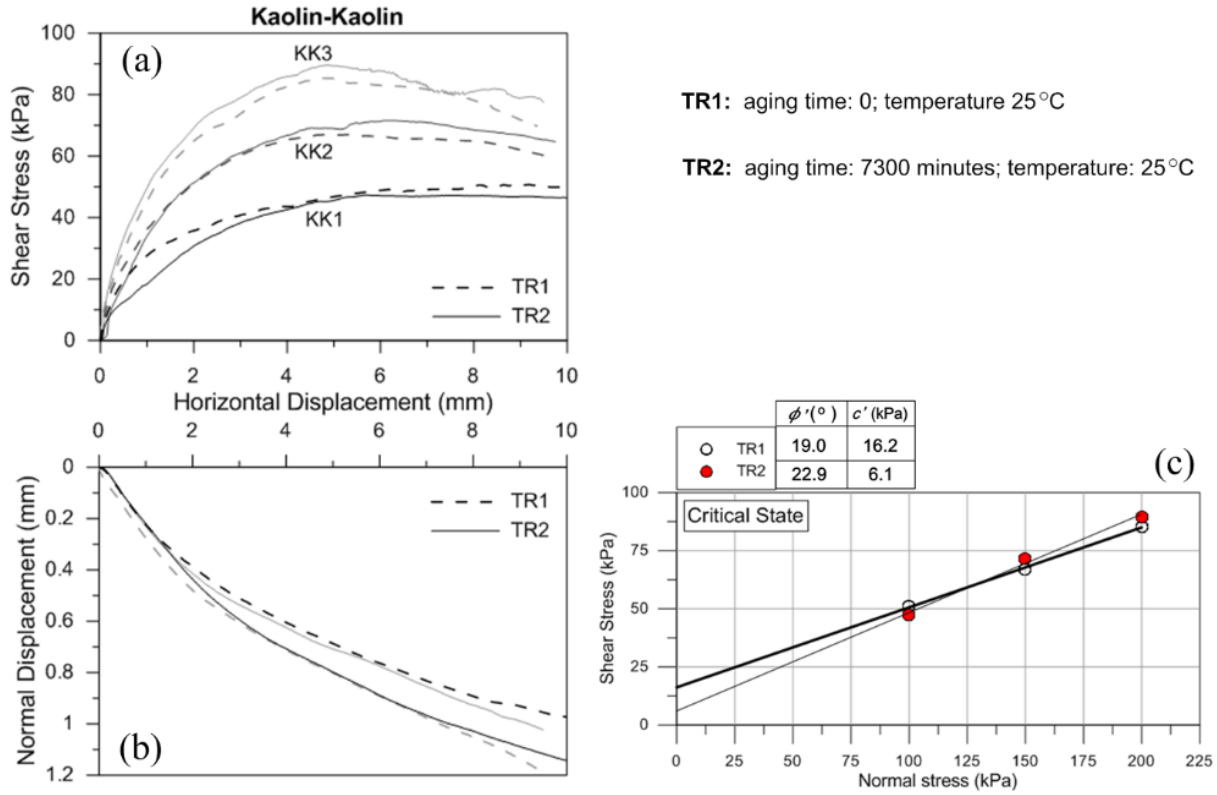

Figure 5-12: Experimental results on NC clay at 25°C: (a) shear stress versus horizontal displacement (b) vertical displacement versus horizontal displacement (c) shear strength envelope

Similar conclusions have been drawn by other researchers on different aging and different reconstituted specimens [14, 37-39]. As time increased to 7300 minutes, the friction angle was positively correlated with the time, but cohesion decreased by 62%. Results on vertical displacement versus horizontal displacement are shown in Figure

5-12(b). In this figure, the clay contracted upon shearing and the shear stress/displacement curves are similar at a given pressure regardless of aging times.

5.4 Consolidated Drained Triaxial Test

5.4.1 Time Effects

The study of time effects was carried out at room temperature as follows. Specimens were consolidated under a confining pressure of 200 kPa. The confining pressure of each specimen was maintained for different periods of time ranging from about 10 hours to 16 days. It should be noted that the primary consolidation, as determined by conventional e – log t plot method, was complete within about six hours. For any given consolidation stress, the value of secondary compression index (C_a) was obtained from the linear portion of the e – log t curve immediately after completion of primary consolidation and the beginning of the secondary consolidation. C_a was calculated as follows:

$$C_a = -\frac{e_t - e_p}{\log(t - t_p)} \qquad 5\text{-}2$$

where $(t_p,\ e_p)$ is the coordinate at the intersection of the tangents to the primary consolidation and secondary parts of the e – log t curve and $(t,\ e_t)$ is the coordinate of the point representing the completion of secondary consolidation on the secondary

compression curve (Figure 5-13)

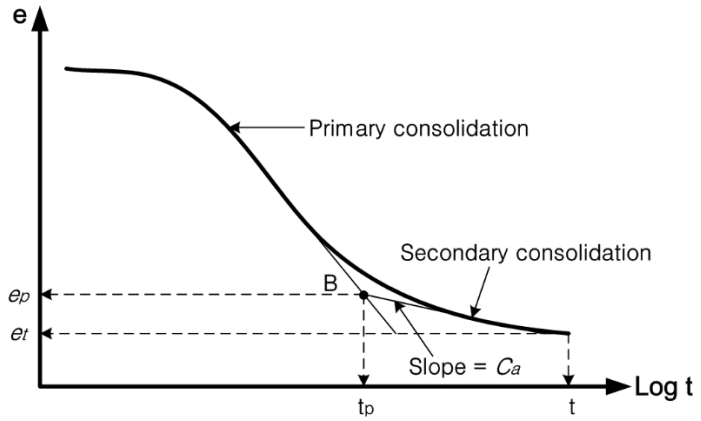

Figure 5-13: A typical *e* – log *t* curve for obtaining the value of C_a [40]

Figure 5-14 shows the creep volume change occurred within 16 days. It is seen from the figure that sample K3-TR2 completed the primary consolidation within 400 minutes of elapsed time (t_p) and the secondary compression index (C_a) derived from result was 0.002928.

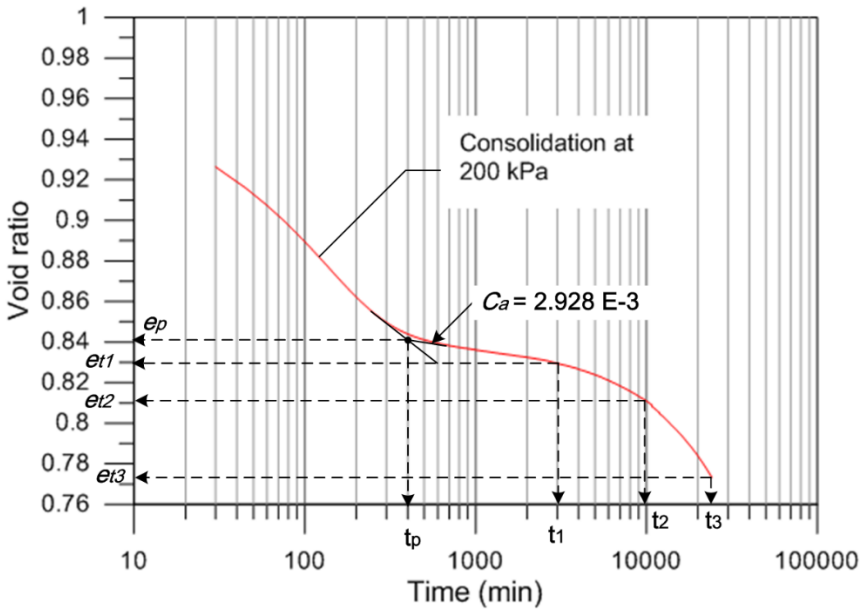

Figure 5-14: Time-induced volume change of Kaolin (specimen No.: K3-TR2)

At constant temperature, however, volume contraction began to reactivate over time. Under the unchanged effective confining pressure, Δe of the sample has a difference between the calculated and the experimental results. The biggest difference occurred at the end of aging (time = 23340 minutes = t_3), and Δe value between t_1 and t_3 is 17 times greater than that obtained by Equation 5-2.

Dependencies of the void ratio, the initial secant modulus (the ratio of shear stress/strain at 0.1% shear strain) and the maximum deviator stress on the consolidation periods derived from the results obtained by the above procedure are presented in Table

5-2.

Table 5-2: Dependencies of void ratio, secant modulus, and maximum deviator stress on consolidation period

Test no.	Consolidation time (minutes)	Void ratio	Secant modulus at 0.1% strain (MPa)	Maximum deviator stress (kPa)
K3-TR	1020	0.836	15.48	294.88
K3-TR2	23340	0.775	12.76	201.05

It clearly shows that the longer the consolidation period the smaller the void ratio; when the consolidation period was increased from 10 hours to 16 days, the void ratio decreased by about 7%. The secant modulus and maximum deviator stress are slightly affected by the consolidation period, the modulus decreased about 18% and the deviator stress decreased about 32%. This suggests that the structure of clay gradually changes with time to produce a new structure, however the new structure is less effective in resisting the subsequent shear distortion which contradicts the results in the direct shear tests (Figure 5-12(c)) and the references [8, 39, 41].

Generally, aging can increase the strength of a clay, for example, as measure by the vane shear test. Bjerrum (1972) [42] recognized this when he started separating the expected, normalized vane shear strength of normally consolidated clays into geologically

young and geologically aged clays. Figure 5-15 suggests an approximate 100% increase in strength at constant plasticity index (PI) due to geologic aging [42].

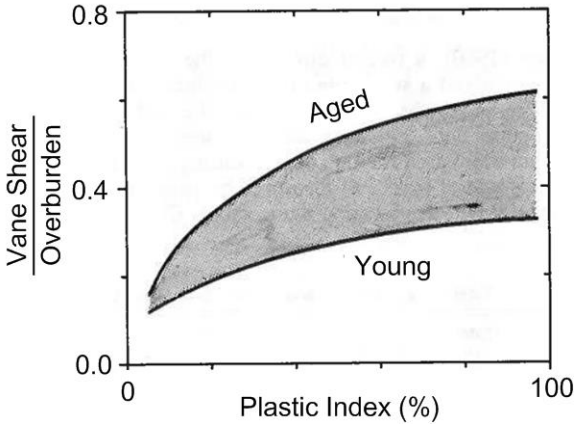

Figure 5-15: Geologic aging increases normalized field vane shear strength in near normally consolidated clays [42]

The strength-increase effect can also occur in clays over engineering aging time in the laboratory. The example in Figure 5-16 from work by Yasuhara and Ue (1983) shows an approximate 50% increase in undrained, direct shear strength with secondary aging time varying from 30 minutes to 30 days [43].

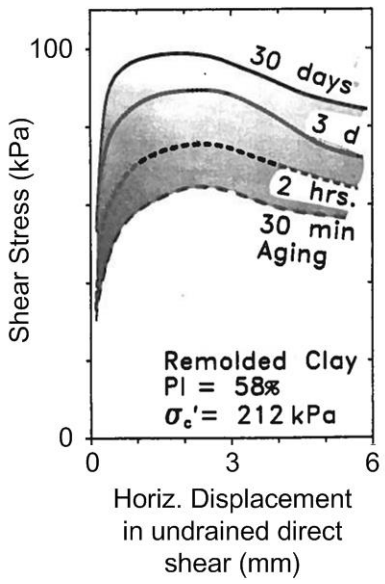

Figure 5-16: Example of laboratory increase in undrained strength of clay due to aging in secondary compression [43]

Under drained condition, direct shear strength in section 5.3.3 presented similar data. Therefore, when appropriate, perhaps more triaxial tests are suggested to carry out and repeat to validate this result. It should be noted that, in the study of temperature effects, the final consolidation pressure for each specimen was maintained about 16 days. Thereafter, the study of time effects revealed that these differences in testing times were likely to have effect on the behavior of the specimens.

5.4.1 Temperature Effects on Normally Consolidated Clay

Procedures for carrying out this investigation were as follows. Specimens were first

consolidated in the triaxial cell under one of the two confining pressures (275 and 325 kPa), and the specimens were subjected to different thermal loads. Thereafter, the specimens were sheared in a drained manner.

For effective confining pressures of 150 kPa, the backpressure of the samples was maintained at 125 kPa, while the confining pressure increased from 125 to 275 kPa; for effective confining pressures of 200 kPa, the backpressure of the samples was maintained at 125 kPa, while the confining pressure increased from 125 to 325 kPa. The specimens were then kept 1020 minutes at effective pressure of 150 and 200 kPa. Thereafter, the thermal controlling unit was switched on at 1020 minutes to perform the heating/cooling cycles on specimens. The following paragraphs describe the details of thermal-induced volume changes together with shear test results. Figure 5-17 shows the void ratio of the sample versus time, as recorded during the 36 heating/cooling cycles of sample K3-TC.

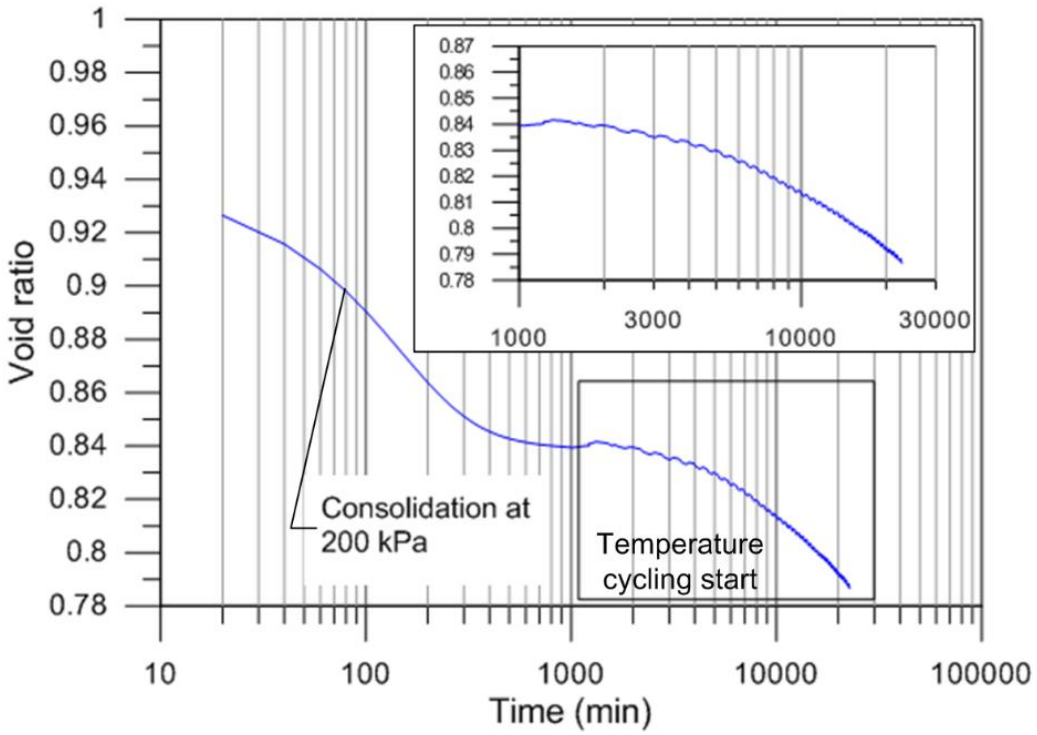

Figure 5-17: Temperature-induced volume change of Kaolin (specimen No.: K3-TC)

It is seen from Figure 5-17 that the primary consolidation was completed within 400 minutes of elapsed time, and the heat pump was switched on at 1020 minutes to perform the heating/cooling cycles on the sample. The temperature of the clay sample was gradually reduced from 22°C through 15°C and down to 5°C. The test results illustrate the volume change caused by temperature cycling. It is seen that the volume contraction was reactivated by temperature cycling, although it had nearly ceased at the end of the primary consolidation.

Since the consolidation of saturated cohesive soils is the result of expulsion of the water that occupies the void spaces or the plastic adjustment of soil fabric [25], the results of thermally induced pore water will be described in this section. The thermally induced pore water pressure is generated due to the difference in the thermal expansion coefficient of water and soil solids. Because the thermal expansion coefficient of water is approximately six times that of clay particle (γ_{clay} = 3.5E-5/℃; γ_{water} = 2.14E-4/℃), the thermal contraction of clay particles is lower than that of water on cooling. Therefore, if the current temperature is lower than the initial temperature, pore water pressure will be lower than the initial value. On the contrary, the pore water pressure will be greater than the initial value if the current temperature is higher than the initial temperature. Figure 5-18 is indicative of the detailed test results for which the temperature was varied at the effective confining pressure of 200 kPa.

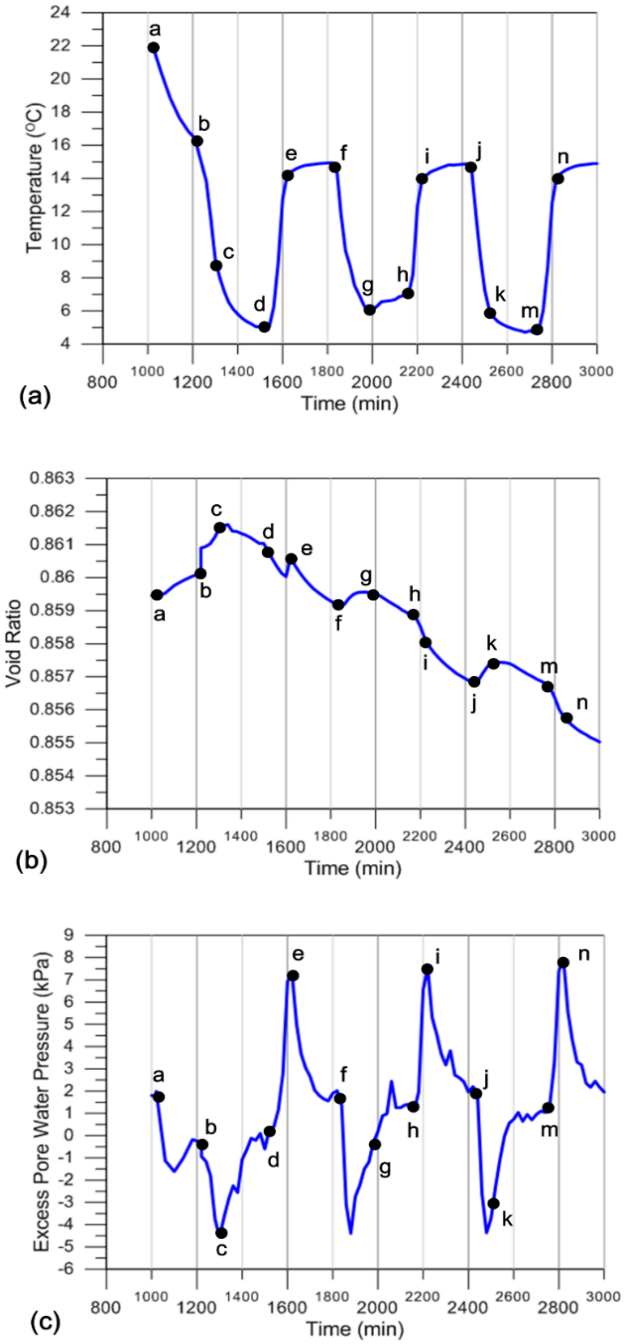

Figure 5-18: Detailed test results of K3-TC in temperature cycling: (a) specimen temperature versus time; (b) volume change versus time; (c) excess pore water pressure versus time

It can be seen from Figure 5-18 that cooling caused the pore water pressure to decrease to a negative value while causing the sample volume to expand (e.g. path f → g and path i → k); On the contrary, the temperature rise during heating caused pore water pressure to increase to a positive value while causing the sample volume to contract (e.g. path h → i and path m → n). During relatively isothermal phases (e.g. path e → f and path g → h), the excess pore water pressure restored to the initial state. Of which, the negative excess pore water pressure was rising to the initial value, and positive excess pore water pressure was decreasing to the initial state. Still, the sample showed a contraction in either of the two processes, indicating that the soil was experiencing plastic deformation.

Thus, the expansion caused by cooling seems to be elastic, so it is reversible if sufficient time is given in the subsequent isothermal phase. In contrast, the contraction caused by heating is irreversible, indicating that the soil is plastically deformed when heated.

Other researchers have reached similar conclusions regarding the non-recoverable contraction during heating for different stresses, different temperature cycling ranges, and

different normally consolidated clays [6, 7, 35, 36]. Possible mechanisms for the drained thermal plastic contraction in normally consolidated soils have been hypothesized to be due to the dissipation of thermally-induced excess pore water pressure resulting from the differential thermal expansion of the soil pore water and soil solids, or due to temperature affecting soil microstructure and thus causing the thermal collapse of the soil skeleton [35]. Recent studies [44] have discovered that the thermally-induced pore water flow on heating can cause the non-recoverable reorientation of the clay particles, which justifies the thermo-plastic macroscale behavior of clays.

The results of the shearing tests are presented in Figure 5-20 and Figure 5-20. The isothermal specimens were prepared using the same procedure as the acyclic and cyclic thermal tests with the exception that the thermal load was omitted. Figure (a) shows diagrams of deviator stress, $\mathrm{q} = (\sigma_1' - \sigma_3')$ versus axial strain, ε_a. Figure (b) displays a diagram of the volumetric strain, ε_v versus axial strain, ε_a.

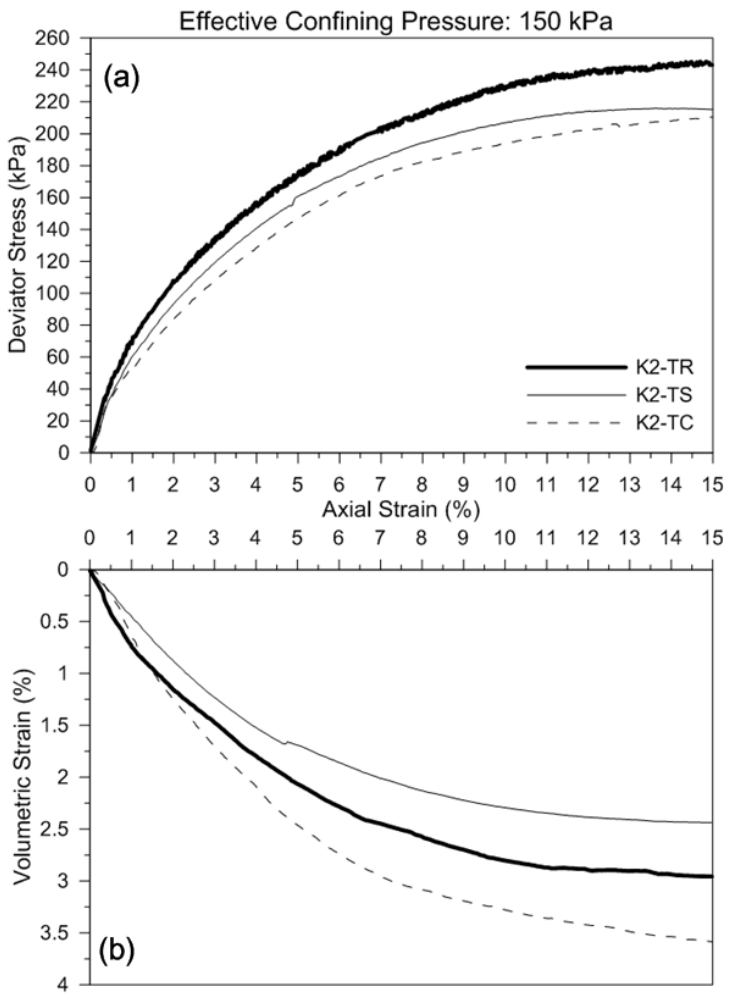

K2-TR: Effective confining pressure: 150 kPa;
Thermal load: N/A

K2-TS: Effective confining pressure: 150 kPa;
Thermal load: acyclic cooling from 25 to 15 °C

K2-TC: Effective confining pressure: 150 kPa;
Thermal load: 36 temperature cycles (5 ⟷15 °C)

Figure 5-19: Results of drained shear test of the NC specimens at 150 kPa

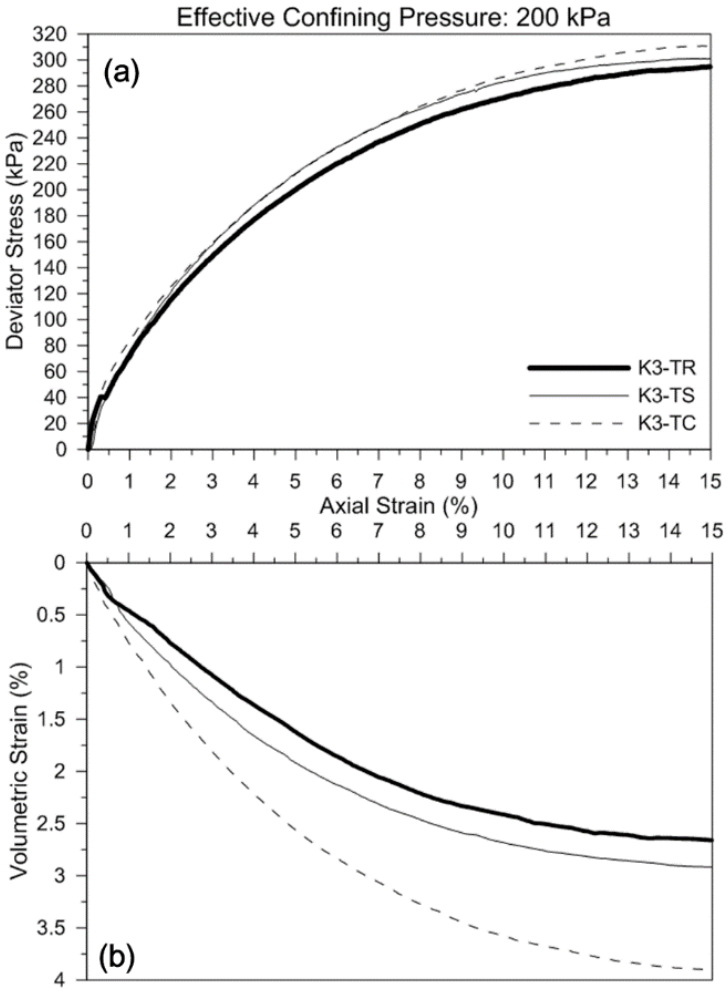

K3-TR: Effective confining pressure: 200 kPa;
Thermal load: N/A

K3-TS: Effective confining pressure: 200 kPa;
Thermal load: acyclic cooling from 25 to 15 °C

K3-TC: Effective confining pressure: 200 kPa;
Thermal load: 36 temperature cycles (5 ⟷15 °C)

Figure 5-20: Results of drained shear test of the NC specimens at 200 kPa

At effective confining pressure of 150 kPa, Figure 5-19 shows that: (1) shear strength and stiffness of thermally-loaded specimens are lower than the isothermal specimen; (2)

cyclic thermally-loaded specimen had the lowest shear strength and stiffness; (3) specimen undergoing heating/cooling cycles shows more compressibility. At effective confining pressure of 200 kPa, Figure 5-20 shows that: (1) shear strength are not significantly affected by different thermal loads but overall the strengths of thermally-loaded specimens were higher than that of isothermal specimen; and (2) specimen undergoing heating/cooling cycles showed smaller dilatancy, similar to the observations made by Hueckel and Baldi (1990) [45] on heated Pontida clay.

As shown in Figure 5-21, the strength envelope at critical state of NC Kaolin clay at ambient temperature is a straight line, with slope M = 0.43 that corresponds to a friction angle of $\phi' \approx 25°$. Figure 5-21 combines the results of drained shear tests at critical state obtained from different thermal loading cases (15°C and 36 heating/cooling cycles). It is shown that the shear strength envelope at critical state is independent of testing thermal loads indicating that the critical-state friction angle is independent of thermal loading for the range of temperature and heating/cooling cycling used herein. This finding is consistent with the written literature (Burghignoli et al. (2000) [7], Cekerevac and Laloui (2004) [11], and Yazdani (2019) [16]).

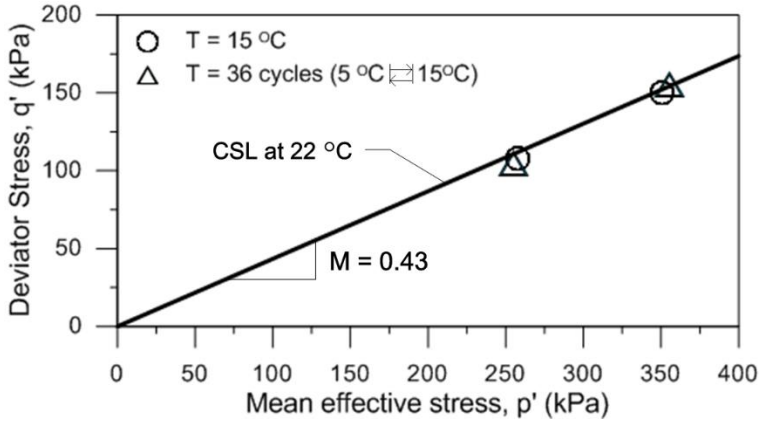

Figure 5-21: Friction angle at critical state for different thermal loads

Details of the void ratio, the initial secant modulus (at 0.1% shear strain) and the maximum deviator stress on the thermal-loaded samples derived from the results are presented in Table 5-3.

Table 5-3: Void ratio, secant modulus, and maximum deviator stress of thermal-loaded specimens

Test no.	Void ratio before thermal load	Void ratio after thermal load	Secant modulus at 0.1% strain (MPa)	Maximum deviator stress (kPa)
K2-TR	0.847	–	10.46	245.24
K2-TS	0.847	0.848	12.41	213.18
K2-TC	0.846	0.835	11.80	207.22
K3-TR	0.836	–	15.48	294.88
K3-TS	0.840	0.842	10.15	301.18
K3-TC	0.840	0.786	13.31	310.98

It can be observed from the Table that cyclic thermal loads result in a minor decrease in void ratio for NC specimens, but the thermally induced volume change seems

independent of elastic secant moduli. In addition, if the void ratio before shear was larger, the specimen with an effective confining pressure of 150 kPa showed greater shear strength, while the specimens with the effective confining pressure of 200 kPa showed completely opposite results. At first glance, the change in shear strength of thermal-loaded specimens in triaxial test may not be pronounced. However, if it is assumed that the reduction of strength caused by aging as described in Section 5.4.1 is reliable, then the cyclic heating and cooling has reduced the shear strength loss due to aging.

5.4.2 Temperature Effects on Over-Consolidated Clay

The effective confining pressure was 50 kPa, and procedures for carrying out this investigation were as follows. Specimens were first consolidated in the triaxial cell under the confining pressure of 175 kPa and the backpressure of 125 kPa, and the specimens were subjected to different thermal loads. Thereafter, the specimens were sheared in a drained manner. The over consolidation rate (OCR) of the specimens herein is 2 since the pre-consolidation pressure of specimens was 100 kPa (for details see Section 4.4.1). Figure 5-22 shows the void ratio of the sample versus time, as recorded during the 36 heating/cooling cycles of sample K1-TC.

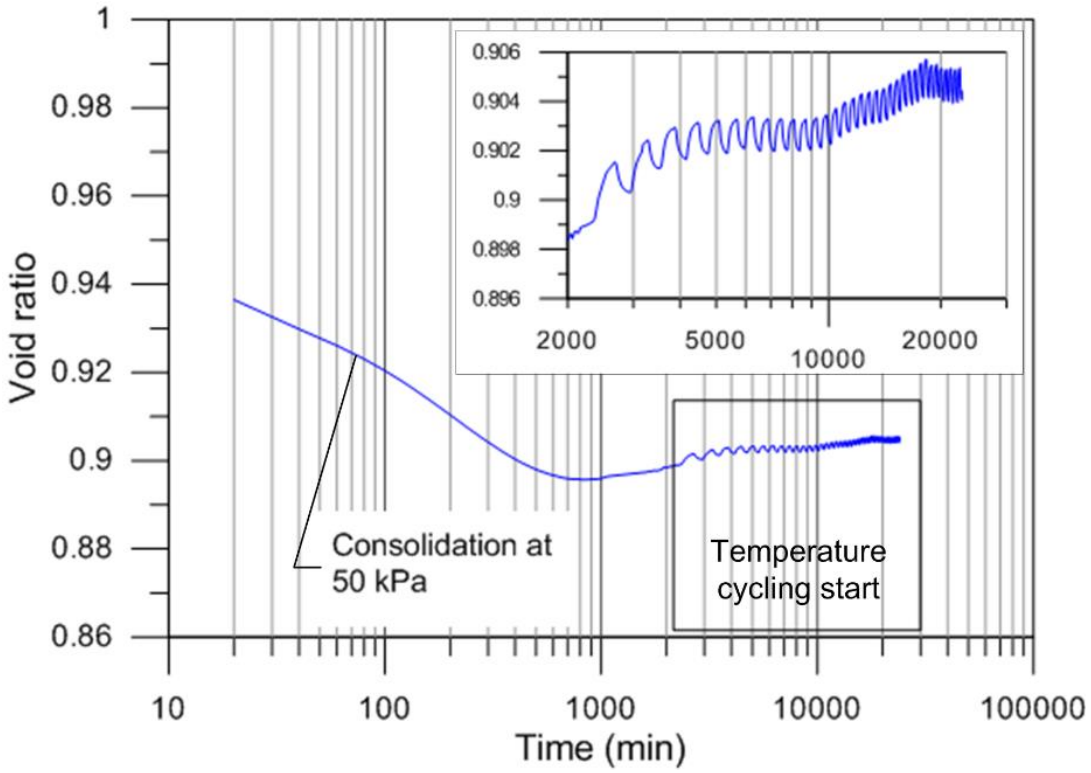

Figure 5-22: Temperature-induced volume change of over-consolidated Kaolin, OCR = 2 (specimen No.: K1-TC)

It is seen from Figure 5-22 that the primary consolidation was completed within 500 minutes of elapsed time, and at about 1000 minutes, the volume compression stopped and the volume began to expand (dilate). Over time, the volume of the over-consolidated specimen is slightly larger than the volume after primary consolidation. The heat pump was switched on at 2140 minutes to perform the heating/cooling cycles on the sample. The temperature of the clay sample was gradually reduced from 22°C through 15°C and

down to 5°C. Figure 5-23 illustrate the volume fluctuation during thermal cycling.

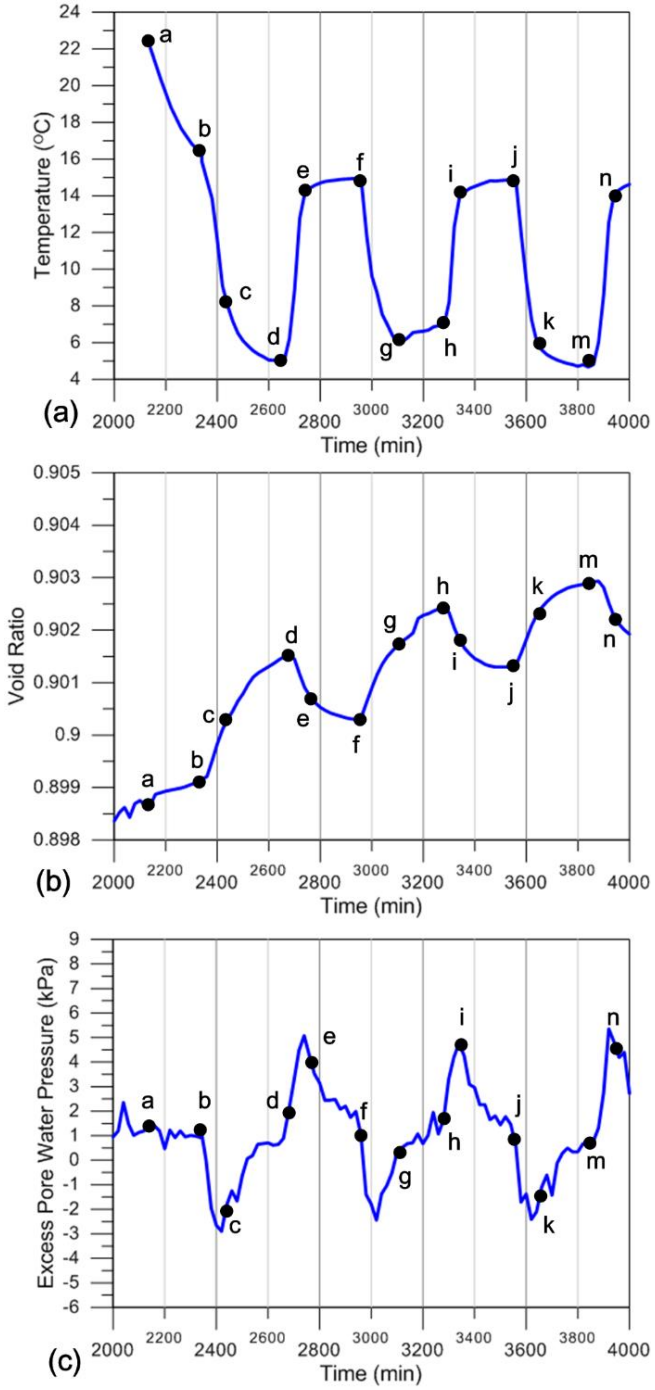

Figure 5-23: Detailed test results of K1-TC in temperature cycling: (a) specimen temperature versus time; (b) volume change versus time; (c) excess pore water pressure versus time

Figure 5-23 is indicative of the detailed test results for which the temperature was varied at the effective confining pressure of 50 kPa. It can be seen from the figure that cooling caused the pore water pressure to decrease to a negative value while causing the sample volume to expand (e.g. path b → c and path j → k); On the contrary, the temperature rise during heating caused pore water pressure to increase to a positive value while causing the sample volume to contract (e.g. path h → i and path m → n). During relatively isothermal phases (e.g. path e → f and path k → m), the excess pore water pressure restored to the initial state. Of which, the negative excess pore water pressure was rising to the initial value, and positive excess pore water pressure was decreasing to the initial state. The volume expansion rate in the cooling isothermal phase tends to slow down (e.g. path k → m), and the volume contraction rate in the heating isothermal phase of also tends to decrease (e.g. path e → f).

Lightly over-consolidated samples exhibiting contraction in drained heating has been discovered by other researchers [6, 11, 46, 47]. In addition, Cekerevac and Laloui (2004) [11] heated Kaolin samples with different stress histories to investigate the relationship between OCR and thermally-induced volume change. They indicated that lightly over-

consolidated samples showed smaller contraction compared with the normally-consolidated samples, and observed that the expansion (dilation) increased with an increase in OCR.

From Figure 5-23, the contraction caused by heating and the expansion caused by cooling appear to partially recover in the lightly over-consolidated specimen. In addition, the volume increase in cooling was slightly greater than the decrease in heating, so the general volume was increased (dilation) after the cyclic thermal loading. Since the cooling-induced dilation in lightly over-consolidated sample is significant, it was concluded that small-amplitude temperature cycling on lightly over-consolidated sample is less likely to cause irreversible volumetric contraction upon heating. However, similar studies on natural clayey soils are recommended for predicting the long-term behavior of thermally loaded soils.

Figure 5-24 (a) shows the results of triaxial tests in the deviator stress versus axial strain plane. The figure indicates that the shear strength of the thermally-loaded specimens are lower than that the isothermal specimen.

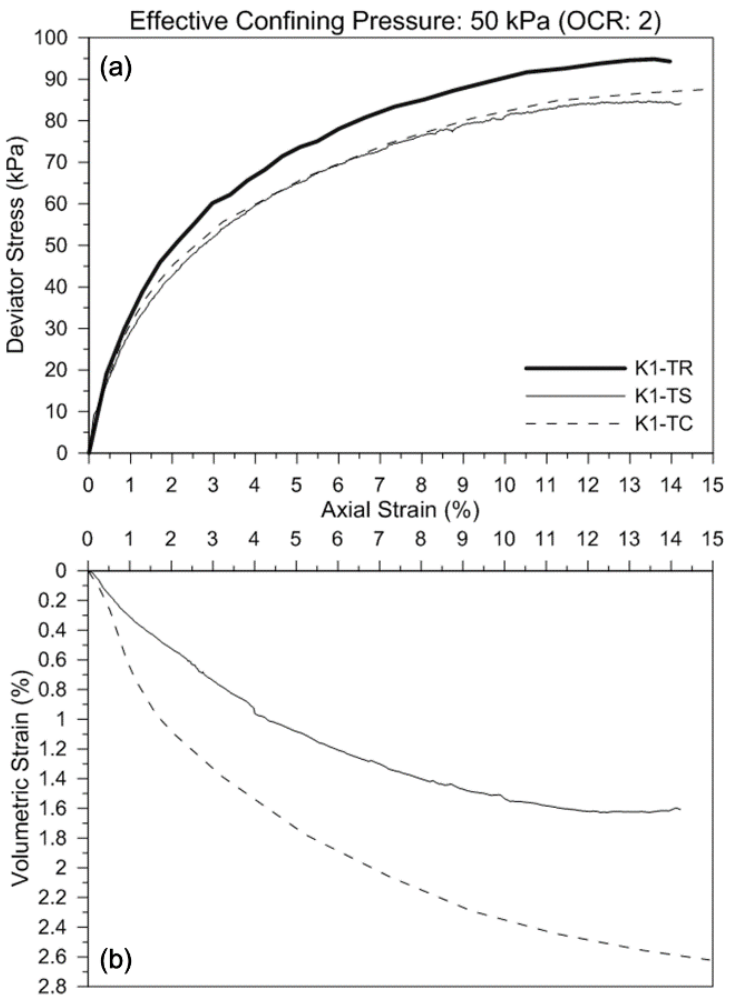

K1-TR: Effective confining pressure: 50 kPa;
Thermal load: N/A

K1-TS: Effective confining pressure: 50 kPa;
Thermal load: acyclic cooling from 25 to 15 °C

K1-TC: Effective confining pressure: 50 kPa;
Thermal load: 36 temperature cycles (5 ⟷15 °C)

Figure 5-24: Results of drained shear test of the OC specimens at 50 kPa

Figure 5-24 (b) shows the volumetric strain of the clay specimen undergoing cyclic thermal loading. The specimen exhibited more compressibility which is similar to the trend

of NC specimens (Figure 5-19 and Figure 5-20). Details of the void ratio, the initial secant modulus (at 0.1% shear strain) and the maximum deviator stress on the thermal-loaded specimens derived from the results are presented in Table 5-4.

Table 5-4: Void ratio, secant modulus, and maximum deviator stress of over-consolidated specimens

Test no.	Void ratio before thermal load	Void ratio after thermal load	Secant modulus at 0.1% strain (MPa)	Maximum deviator stress (kPa)
K1-TR	0.896	–	6.28	94.83
K1-TS	0.899	0.902	5.55	84.81
K1-TC	0.899	0.903	6.48	87.59

As can be seen from Table 5-4, the thermally-loaded OC specimens have undergone minor volumetric expansion. The shear strength decreased slightly with the increase of void ratio before shearing, but the elastic secant modulus does not seem to be affected by volume change. Thermally induced swelling can occur on heated OC clays [8, 48] and is interpreted as that heated OC specimens are looser than unheated ones, so the macro-resistance of OC clay should be expected to decrease with increasing temperature [8]. However, lightly over-consolidated clays usually contract on heating and cyclic heating/cooling [6, 11, 46, 47]. These references have found that shear strength will rise if the sample undergoes thermally induced compression. Whereas, the experiments in this study found that if the temperature rise is small, the contraction caused by heating on

the lightly OCR sample is reversible. As swelling caused by cooling and aging may lead to reduced shear strength, it may be suggested that small-amplitude heating may play a compensation role in affecting the mechanical properties of lightly OCR clay.

Chapter 6

Effects of Cyclic Temperature Changes on the Drained Shear Strength of Clay and on the Side Resistance of Clay-Concrete Interface

6 Discussion

6.1 Effect of Temperature Cycling on Soil Mechanical Behavior

This section discusses the relationship between the strength and the volume changes induced by the small-amplitude thermal load. At this stage only qualitative, not quantitative, evaluation of such relationship can be carried out since the tests on clay with heating/cooling cycling and aging are time consuming, only one test has been conducted at each temperature and stress level. In the drained consolidated triaxial tests, the function of effective mean stress and deviator stress are linear relationship, and in slow direct shear tests, the relationship between the shear strength and the normal stress can be well correlated with a linear function which allows determining the friction angle and the cohesion. These observations show equally the reliability of the obtained results.

To analyze the effect of temperature on the friction angle of Kaolin clay, the results of the present work are combined with those of other authors ([7, 11, 16, 17, 45, 49, 50]) in the same figure (Figure 6-1). The results of existing studies show that the effect of temperature on friction angle of clay is controversial. At higher temperatures, the friction angle may be higher in some cases and lower in other cases. Regarding the effect of

cyclic thermal load on friction angle, Yazdani (2019) [16] and the present investigation found that the friction resistance of NC Kaolin clay increased slightly after thermal cycling (2.0° to 3.3°). However, present research on aged Kaolin clay also shows similar increases, so it is not yet possible to attribute all the increase in friction angle to temperature effect alone.

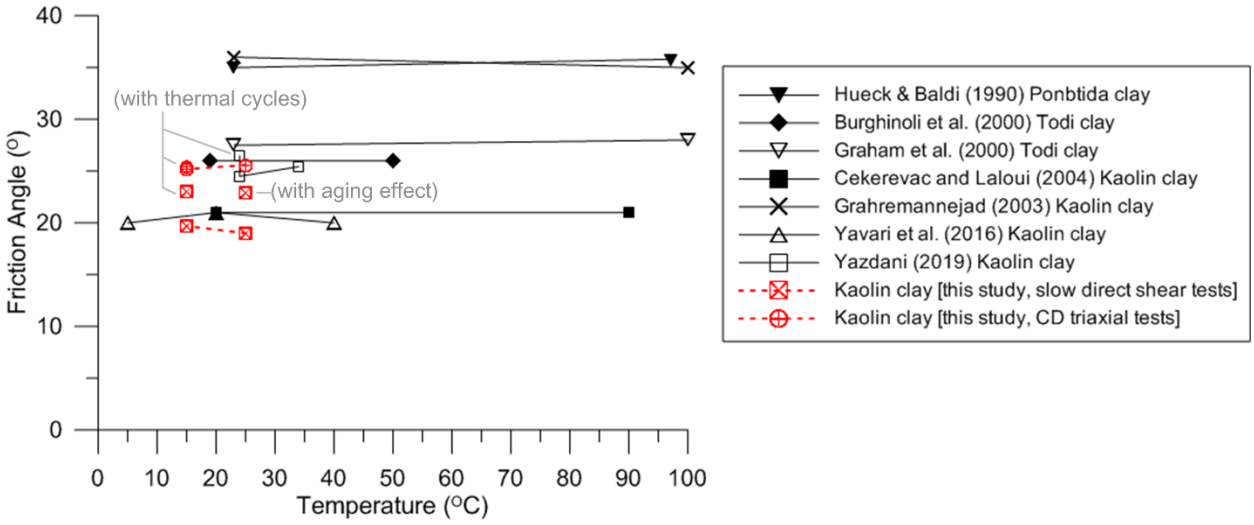

Figure 6-1: Effect of temperature on friction angle

Shear deformation of clay can be explained through toe aspects: micro-resistance and macro-resistance. Micro-resistance is the resistance arising from bonding at inter-particle contacts (solid and solid); macro-resistance, on the other hand, is the resistance induced by movement of clay particles over other particles within the shear plane.

When clay particles are brought into contact, the absorbed water around clay particles is a barrier against the formation of the inter-particle contacts [51, 52]. During the consolidation process, the absorbed water may be squeezed out of the contact points because the irregularities of the particle surface cause the actual stresses at the contact points to be much higher than the applied stresses [53].

Soil creep may cause an increase in inter-particle contacts. The increase in the contacts can be explained by the fact that the strength of the absorbed water barrier around the clay particles decreases over time, and that can be accelerated by the heating/cooling cycles [48, 54].

Microscopic studies performed by Pusch and Güven (1990) [55] on Na-bentonite at elevated temperatures have shown irreversible microstructure rearrangement in the form of denser flakes which are normally associated with permanent increased in the mechanical strength and stiffness [13]. In addition, recent microscopic studies performed by Jaradat et al. (2018) [44] find unrecoverable reorientation on Kaolinite particles during heating/cooling and they further indicate that the rearrangement is highly dependent on the direction of the initial orientation of clay particles with respect to the thermal gradient.

Thus, the micro-resistance of clay should increase upon aging and the rate of increase may be accelerated by heating/cooling cycling.

The magnitude of macro-resistance depends on many factors, including clay fabric, packing, and effective confining pressure (Sivakumar et al. (2002) [56]). As time passed, the direction and the texture of soil fabrics became disoriented (Mitchelle et al. (1965) [57]) and rigid (Allam and Sridharan (1979) [58]). A disoriented fabric yields a stiffer stress-strain response and higher shear strength than an oriented fabric (Seed et al. (1960) [59]); a rigid fabric has less failure strain than a soft texture [58]. In addition to the time effect, most literature have results of NC and lightly OC clays exhibiting contraction on heating and heating – cooling cycle [11-13], and exhibiting greater shear strength than the unheated specimens. Kuntiwattanakul et al. (1995) [8] had proposed that if the temperature changes cause the volume to compress, the macro-resistance of the clay will increase, but if the temperature changes cause the volume to expand, the macro-resistance will decrease.

6.2 Effect of Temperature Cycling on Side Resistance of Energy Pile

In the process of interface shearing, Tsubakihara and Kishida (1993) [60] obtained

two failure modes through direct shear tests on clay and steel plate which is determined by roughness of interface. When the steel surface was smoother than the critical roughness, slip failure occurred, followed by the reduction in frictional resistance. In contrast, if the steel roughness exceeded the critical value, elastic-plastic failure occurred within clay specimen, so that the maximum resistance of friction agreed with shear strength of clay.

In the present study, since the same concrete slab was used in all direct shear tests, it was assumed that the roughness of the concrete surface unchanged regardless the repeated use. If the roughness of the concrete surface is assumed to stay the same, the thermally induced changes in friction coefficient are attributed to the thermo-mechanical behavior of clay near the interface.

According to section 6.1 and literature, NC clay near the interface is irrecoverably strengthened during temperature cycling. Jaradat et al. (2017) [5] used X-ray diffraction experiments to study the microstructure of Kaolin clay. They found that particles of Kaolin clay are irreversibly rearranged under heating and cooling. Therefore, the interface is expected to show higher resistance to shear deformation.

Stiff clay-concrete interface is generally expected to present slip failure mode unlike soft clay-concrete interface, due to the fact that a shear zone is more difficult to be formed within a stronger clay. Therefore in the direct shear tests, the results in Figure 5-8(a) can be interpreted as the clay is strengthened under cyclic thermal load, which increases the frictional resistance coefficient ($\tan\delta$) at the interface. Similarly, the decrease in ductility of the shearing interface shown in Figure 5-7(a) is due to the increase in stiffness of clay. However, regarding ultimate resistance as shown in Figure 5-8(b), the residual friction coefficient appears not related to the thermal history of the interface.

The analysis of pile's side friction is based on the principle of sliding friction. The direct shear test for soil-concrete interface is a standard method for obtaining friction resistance coefficient of a concrete pile in ground. In this section, the data collected from direct shear tests are applied to the empirical formulas to calculate axial load capacities of the model piles. The results are then compared with the results of the small-scale pile tests.

In effective stress analysis, a simple sliding-friction model can be describe by Equation 4.2 ($f_s = \beta\sigma_z'$) in Section 4.1.3. Where f_s is unit side-friction resistance, σ_z' is effective overburden stress, and β is the Bjerrum-Burland coefficient. In Section 4.1.3,

an empirical value for soft clay (in Table 4-1) was employed to estimate the gross load capacity of the model-scale pile before testing.

The peak fiction angle of the soil-concrete interface (δ) under different histories are available in Section 5.2, and the peak fiction angle of the soil (ϕ') under different histories are available in Section 5.3. Therefore, in this section the Bjerrum-Burland coefficient can be calculated by empirical equation as follow:

$$\beta = K_0(\frac{K}{K_0})\tan\delta \qquad 6\text{-}1$$

where

$\tan\delta$ = μ = coefficient of friction between the soil and the foundation

δ = soil-foundation interface friction angle

K = σ_h'/σ_v' = coefficient of lateral earth pressure after construction

K_0 = $\sigma_{h0}'/\sigma_{v0}'$ = coefficient of lateral earth pressure before construction

In Equation (6-1), $\frac{K}{K_0}$ ratio depends on construction techniques, in Table 6-2 is the approximate ratio of coefficient of lateral earth pressure after construction to that before construction. This research adopted $\frac{K}{K_0}$ ratio is 0.60 as the small-scale pile test was

prepared with the pre-installed pile and kaolin slurry.

Table 6-1: Approximate ratio of coefficient of lateral earth pressure after construction to that before construction [61]

Foundation Type and Method of Construction	$\frac{K}{K_0}$
Pile—jetted	0.5–0.7
Pile—small displacement, driven	0.7–1.2
Pile—large displacement, driven	1.0–2.0
Drilled shaft—built using dry method with minimal sidewall disturbance and prompt concreting	0.9–1.0
Drilled shaft—slurry construction with good workmanship	0.9–1.0
Drilled shaft—slurry construction with poor workmanship	0.6–0.7
Drilled shaft—casing method below water table	0.7–0.9

In Equation (6-1), the value of coefficient of lateral earth pressure in undisturbed ground is known as the coefficient of lateral pressure at rest (K_0). The values of K_0 are between 0.35 and 0.7 for normally consolidated soils (Conduto (2001) [25]).The most common method of accessing K_0 is by using empirical correlations with soil properties. Following is a widely used formula developed by Mayne and Kulhawy (1982) [62]:

$$K_0 = (1 - \sin\phi')\mathrm{OCR}^{\sin\phi'} \qquad 6\text{-}2$$

Where OCR is over-consolidation ratio that is defined as the ratio of current pressure to

pre-consolidation pressure. The value of OCR for normally consolidated soils is 1.0. While ϕ' is effective friction angle of soil. The effective friction angle of Kaolin under the same stress and thermal history can be obtained from Figure 5-12 and Figure 5-12. Thus, K_0 for each thermal loading path is obtained from Equation (6-2) (see Table 6-2).

Table 6-2: Allowable compressive load capacity of model pile (referred to Equation 4-2, Equation 6-1 and Equation 6-2)

Case	$\tan\delta$	ϕ′ (°)	K_0	β	σ_z' (kPa)	f_s (kPa)	A_s (mm²)	P_s (N)	W_f (N)	$Q_{ult\text{-}calculated}$ (N)	$Q_{ult\text{-}measured}$ (N)
TR	0.37	19.0	0.67	0.15	100	14.87	14,187	211	2.3	209	123
TS	0.33	19.7	0.66	0.13	100	13.07	14,187	185	2.3	183	117
TC1	0.37	22.4	0.62	0.14	100	13.76	14,187	195	2.3	193	–
TC2	0.43	23.0	0.61	0.16	100	15.74	14,187	223	2.3	221	53

Note: TR, isothermal at 25°C; TS: acyclic cooling; TC1: 10 heating/cooling cycles; TC2: 36 heating/cooling cycles; $\boldsymbol{\tan\delta}$, coefficient of friction between soil and foundation; $\boldsymbol{\sigma_v'}$, effective vertical stress; $\boldsymbol{\phi'}$, effective friction angle of soil; $\boldsymbol{K_0}$, lateral earth pressure coefficient; $\boldsymbol{f_s}$, unit friction resistance; $\boldsymbol{A_s}$, side-friction contact area of foundation; $\boldsymbol{P_s}$, side-friction resistance; $\boldsymbol{W_f}$, weight of foundation; $\mathbf{Q}_{ult\text{-}calculated}$, the calculated pile gross axial load capacity; $\mathbf{Q}_{ult\text{-}measured}$, the measured pile gross axial load capacity.

Table 6-2 lists the calculated unit side friction (f_s) and the calculated pile gross axial load capacity, $Q_{ult\text{-}calculated}$, based on the results of direct shear tests performed in this study. The table also includes the measured pile gross axial load capacity, $Q_{ult\text{-}measured}$. A direct comparison between the measured and calculated pile capacities indicate that

directly employing the friction coefficient will result in an overestimation on the friction resistance of the model pile. In case TC1, there is no small-scale pile results on this stage to validate the calculated pile gross axial load capacity ($Q_{ult\text{-}calculated}$). In case TR and case TS, the ratio of $Q_{ult\text{-}calculated}/Q_{ult\text{-}measured}$ is 1.56 and 1.70, respectively.

The difference between $Q_{ult\text{-}calculated}$ and $Q_{ult\text{-}measured}$ may be attributed to (1) skin friction in clay soils is due to adhesion between the pile material and clay (Rajapakse (2016) [63]), and (2) $Q_{ult\text{-}calculated}$ is based on the effective friction resistance in long-term condition, but the $Q_{ult\text{-}measured}$ obtained from the small-scale pile test that did not fully achieve drained condition in the entire procedure (e.g. the rate of heating/cooling cycles was not adequate for the drained conditions, and the axial loading condition was not slow enough to satisfy drained conditions).

From Table 6-2, the difference between $Q_{ult\text{-}measured}$ and $Q_{ult\text{-}calculated}$ for case TC2 is significant. As explained earlier (Section 5.1.3), the freeze-thaw cycles are reponsinle for the tremendous loss of pile loading capacity. The freeze-thaw cycles only occurred in the small-scale pile test, and not in the slow direct shear test and the slow Kaolin-concrete interface direct shear tests, therefore $Q_{ult\text{-}measured}$ is much smaller than $Q_{ult\text{-}calculated}$.

Chapter 7

Conclusions

7 Conclusion

This research used laboratory tests and small-scale pile tests to investigate temperature effect on engineering behavior of clay and clay-concrete interface, and precisely how intermittent operation of geothermal pump in cold weather affects soil creep and interface friction angle. Moreover, soil aging tests were performed to provide another perspective when analyzing long-term laboratory test results. The main conclusions of this investigation are:

(1) Temperature cycling under drained conditions causes ductility of the NC clay-concrete interface to decrease. Under drained conditions, although the residual interface friction angle of NC clay with concrete is independent of temperature, the peak interface friction angle increases with heating/cooling cycles.

(2) Accordingly, the pile's side friction increases with heating/cooling cycles. The adhesion of NC clay with concrete, however, shows a downward trend with the heating/cooling cycles.

(3) Two small-scale pile tests, one isothermal pile (25°C) and one acyclic cooled pile (soil at pile surface was cooled from 25°C to 18°C) failed under similar axial loads. However,

the third pile that was subjected to 36 heating/cooling cycles failed prematurely at a very small axial load. This was due to soil fatigue caused by repeated freeze-thaw cycles that occurred around the pile.

(4) In the small-scale pile tests, directly using the effective friction coefficients obtained from the Kaolin-Concrete interface direct shear tests to estimate the pile gross axial load capacities is not feasible because the two tests have different conditions. However, using the empirical β method and assuming the Bjerrum-Burland coefficient of the Kaolin specimen is 0.15 can achieve a value that is relatively closer to the actual pile gross axial load capacity in the small-scale pile test (e.g. case TR).

(5) Normally consolidated clay expands with cooling and contracts with heating. The volumetric strain during cooling is elastic within the testing temperatures, but the deformation during heating is a combination of elastic and plastic strains. Compared to the unheated specimens, the secondary compression of the cycle thermal loaded ones is significant. Other researchers have found similar behavior in heated soils and described this volume change behavior as accelerated creep. Recent research [44] found that heating causes the non-recoverable reorientation of the clay particles,

which justifies the thermo-plastic macroscale behavior of clays.

(6) Thermal volumetric strain depends on the stress history (over-consolidation ratio). At cooling state, this research found that contraction which was caused by heating is reversible in lightly over-consolidated clays. Besides, the total volume change of lightly over-consolidated Kaolin in the thermal cycles was expansion as the volume expansion during cooling is more significant than contraction during heating.

(7) In slow direct shear tests, more heating/cooling cycles caused the clay to behave a more ductile mechanical behavior. The cyclic thermal loaded specimen exhibited a higher shear resistance in the tests. At larger shear displacement when the critical state is reached the shear stress drops and has almost the same value as the one obtained from samples tested at constant temperature. Although the friction angle at critical state seems to be independent of test temperature, it increases with the number of test thermal cycles.

(8) In consolidated drained triaxial tests, dilatancy of the cyclic thermal loaded samples significantly decreased regardless of stress history. However, shear strength seems to depend on the current stress level. For over-consolidated state or with small

confining pressure, the deviator stresses of cooled and cyclic thermal loaded specimens are lower than that of isothermal ones while the opposite result is observed at relatively higher confining pressures.

(9) This study found that the friction angle of Kaolin clay increased with the increase of aging, and the friction angle of the specimen aged under constant temperature was equivalent to that of the specimen subjected to thermal cycling. However, this result may be due to the temperature range being too small ($\Delta T = 10℃$) to have a significant temperature effect.

8 References

[1] H. Brandl, "Energy foundations and other thermo-active ground structures," *Géotechnique,* vol. 56, pp. 81-122, 2006.

[2] E. Kikuchi, D. Bristow, and C. A. Kennedy, "Evaluation of region-specific residential energy systems for GHG reductions: Case studies in Canadian cities," *Energy Policy,* vol. 37, 2009.

[3] C. Knellwolf, H. Peron, and L. Laloui, "Geotechnical Analysis of Heat Exchanger Piles," *J. Geotech. Geoenviron. Eng.,* vol. 137, pp. 890-902, 2011.

[4] M. Faizal, A. Bouazza, and R. M. Singh, "An experimental investigation of the influence of intermittent and continuous operating modes on the thermal behaviour of a full scale geothermal energy pile," *Geomechanics for Energy and the Environment,* vol. 8, pp. 8-29, 2016.

[5] K. A. Jaradat, Z. Darbari, M. Elbakhshwan, S. L. Abdelaziz, S. K. Gill, E. Dooryhee*, et al.*, "Heating-freezing effects on the orientation of kaolin clay particles," *Applied Clay Science,* vol. 150, pp. 163-174, 2017.

[6] G. Baldi, T. Hueckel, and R. Pellegrini, "Thermal volume changes of the mineral-

water system in low-porosity clay soils," *Canadian Geotechnical Journal,* vol. 25, 1988.

[7] A. Burghignoli, A. Desideri, and S. Miliziano, "A laboratory study on the thermomechanical behaviour of clayey soils," *Canadian Geotechnical Journal (Revue canadienne de géotechnique),* vol. 37, pp. 764-780, 2000.

[8] P. Kuntiwattanakul, I. Towhata, K. Ohishi, and I. Seko, "Temperature effects on undrained shear characteristics of clay," *SOILS AND FOUNDATIONS,* vol. 35, pp. 147-162, 1995.

[9] P. J. Bourne-Webb, B. Amatya, K. Soga, T. Amis, C. Davidson, and P. Payne, "Energy pile test at Lambeth College, London: geotechnical and thermodynamic aspects of pile response to heat cycles," *Géotechnique,* vol. 59, pp. 237-248, 2009.

[10] L. Laloui, M. Nuth, and L. Vulliet, "Experimental and numerical investigations of the behavior of a heat exchanger pile," *International Journal for Numerical and Analytical Methods in Geomechanics,* vol. 30, pp. 763-781, July 2006 2006.

[11] C. Cekerevac and L. Laloui, "Experimental study of thermal effects on the mechanical behaviour of a clay," *International Journal for Numerical and Analytical*

Methods in Geomechanics, vol. 28, pp. 209-228, March 2004 2004.

[12] H. M. Abuel-Naga, D. T. Bergado, G. V. Ramana, L. Grino, and P. T. Rujivipat, Y., "Experimental Evaluation of Engineering Behavior of Soft Bangkok Clay under Elevated Temperature," *Journal of Geotechnical and Geoenvironmental Engineerin,* vol. 132, pp. 902-910, July 2006 2006.

[13] H. M. Abuel-Naga, D. T. Bergado, and B. F. Lim, "Effect of temperature on shear strength and yielding behavior of soft Bankok clay," *Soils and Foundations,* vol. 47, pp. 423-436, 2007.

[14] J. H. Schmertmann, "The Mechanical Aging of Soils," *Journal of Geotechnical Engineering,* vol. 117, pp. 1288-1330, 1991.

[15] A. Di Donna, A. Ferrari, and L. Laloui, "Experimental investigations of the soil–concrete interface: physical mechanisms, cyclic mobilization, and behaviour at different temperatures," *Canadian Geotechnical Journal,* vol. 53, pp. 659-672, 2015.

[16] S. Yazdani, "Study of the long-term shaft resistance of energy piles in saturated clays," PhD, Civil and Enviromental Engineering, Univesrity of Wisconsin

Milwaukee, Milwaukee, Wisconsin, 2019.

[17] N. Yavari, A. M. Tang, J. M. Pereira, and G. Hassen, "Effect of temperature on the shear strength of soils and the soil–structure interface," *Canadian Geotechnical Journal,* vol. 53, pp. 1186-1194, 2016.

[18] C. W. W. Ng, C. Shi, A. Gunawan, L. Laloui, and H. L. Liu, "Centrifuge modelling of heating effects on energy pile performance in saturated sand," *Canadian Geotechnical Journal,* vol. 52, pp. 1045-1057, 2014.

[19] M. A. Stewart and J. S. McCartney, "Centrifuge Modeling of Soil-Structure Interaction in Energy Foundations," *Journal of Geotechnical and Geoenvironmental Engineering,* vol. 140, April 2014 2014.

[20] X. Huang, Y. Wu, H. Peng, Y. Hao, and C. Lu, "Thermomechanical Behavior of Energy Pile Embedded in Sandy Soil," *Hindawi Mathematical Problems in Engineering,* vol. 2018, 2018.

[21] S. Yazdani, S. Helwany, and G. Olgun, "Investigation of Thermal Loading Effects on Shaft Resistance of Energy Pile Using Laboratory-Scale Model," *J. Geotech. Geoenviron. Eng.,* vol. 145, 2019.

[22] J. S. McCartney and J. E. Rosenberg, "Impact of heat exchange on side shear in thermo-active foundations," in *Geo-Frontiers Congress 2011*, ed. Dallas, Texas, United States, 2011.

[23] O. T. Farouki, *Thermal properties of soils* vol. 81. Hanover, New Hampshire, U.S.A.: United states army corps of engineers cold regions research and engineering laboratory (CRREL), 1981.

[24] D. Pahud and M. Hubbuch, "Measured thermal performances of the energy pile system of the dock midfield at Zürich Airport," in *European Geothermal Congress 2007*, Unterhaching, Germany, 2007.

[25] D. P. Coduto, *Foundation design principles and practices*, 2 ed.: Prentice Hall, 2001.

[26] P. J. Hannigan, G. G. Goble, G. E. Thendean, G. E. Likins, and R. F., "Design and Construction of Driven Pile Foundations," Federal Highway Administration, Washington, DC1997.

[27] J. Burland, "Shaft Friction of Piles in Clay - A simple Foundation Approach," *Ground Engineering,* vol. 6, pp. 30-42, 1973.

[28] W. F. Chen and J. Y. R. Liew, *The Civil Engineering Handbook*: CRC Press, 1995.

[29] C. D. Olmo, V. Fioravante, F. Gera, H. T., J. C. Mayor, and R. Pellegrini, "Thermomechanical properites of deep argillaceous formations," *Engineering Geology,* vol. 41, pp. 87-101, 1996.

[30] A. A. o. S. H. a. T. O. (AASHTO), "AASHTO LRFD Bridge Design Specifications, US Customary Units, Seventh Edition, with 2015 Interim Revisions. ," ed. Washington, D.C.: American Association of State Highway and Transportation Officials, 2014.

[31] A. J. Weltman, "Pile load testing procedures," Construction Industry Research and Information Association, London1980.

[32] ASTM, "Axial Pile Loading Test—Part 1: Static Loading," ed: ASTM, 1985.

[33] B. S. I. (BSI), "British standard code of practice for foundations," in *BS-8004*, ed. London: British Standards Institution (BSI), 1986.

[34] A. Hirany and F. H. Kulhawy, "Interpretation of load tests on drilled shafts," in *Proc., Foundation Engineering: Current Principles and Practices*, 1989, pp. 1132-1149.

[35] R. G. Campanella and J. K. Mitchell, "Influence of temperature variations on soil

behaviour," *Journal of the Soil Mechanics and Foundations,* vol. 94, pp. 709-734, May 1968 1968.

[36] R. L. Plum and M. I. Esrig. Some temperature effects on soil compressibility and pore water pressure [Online]. Available: http://onlinepubs.trb.org/Onlinepubs/sr/sr103/103-022.pdf

[37] T. L. Youd and I. M. e. Idriss, "Proceedings NCEER Workshop on Evaluation of Liquefaction Resistance of Soils," National Center for Earthquake Engineering Research, Buffalo1977.

[38] J. K. Mitchell and Z. V. Solymar, "Time dependent strength gain in freshly deposited or densified sand," *J. Geotech. Eng.,* vol. 110, pp. 1559-1576, 1984.

[39] M. Ltifi, T. Abichou, and J. Tisot, "Effects of Soil Aging on Mechanical and Hydraulic Properties of a Silty Soil," *Geotechnical and Geological Engineering,* vol. 32, pp. 1101-1108, 2014.

[40] C. A. Anagnostopoulos and I. N. Grammatikopoulos, "A new model for the prediction of secondary compression index of soft compressibile soils " *Bull Eng Geol Environ,* vol. 70, pp. 423-427, 2011.

[41] M. M. Allam and A. Sridharan, "The influence of aging on the shear strength behavior of two fine-grained soils," *Canadian Geotechnical Journal,* vol. 16, pp. 391-397, 1979.

[42] L. Bjerrum, "Embankments on soft ground," in *Perfomance of earth and earth supported structures*, Purdue University 1972.

[43] K. Yasuhara and S. Ue, "Increase in undrained shear strength due to secondary compression," *Soils and Foundations,* vol. 23, pp. 50-64, 1983.

[44] K. A. Jaradat, Z. Darbari, M. Elbakhshwan, S. L. Abdelaziz, S. K. Gill, E. Dooryhee*, et al.*, "Heating-Freezing effects on the orientation of kaolin clay," March 2018.

[45] T. Hueckel and G. Baldi, "Thermoplasticity of Saturated Clays: Experimental Constitutive Study," *Journal of Geotechnical Engineering,* vol. 116, December 1990 1990.

[46] P. Delage, N. Sultan, and Y. J. Cui, "On the thermal consolidation of Boom clay," *Canadian Geotechnical Journal,* vol. 37, pp. 343-354, 2000.

[47] H. M. Abuel-Naga, D. T. Bergado, and A. Bouazza, "Thermally induced volume change and excess pore water of soft Bangkok clay," *Engineering Geology,* vol.

89, pp. 144-154, 2007.

[48] I. Towhata, P. Kuntiwattanaku, I. Seko, and K. Ohishi, "Volume change of clays induced by heating as observed in consolidation tests," *Soil and Foundations,* vol. 33, pp. 170-183, 1993.

[49] J. Graham, N. Tanaka, T. Crilly, and M. Alfaro, "Modified Cam-Clay modelling of temperature effects in clays," *Canadian Geotechnical Journal,* vol. 38, pp. 608-621, 2001.

[50] B. Ghahremannejad, "Thermo-mechanical behaviour of two reconstituted clays," University of Sydney, Australia, 2003.

[51] J. K. Mitchell, R. G. Campanella, and A. Singh, "Soil Creep As A Rate Process," *Journal of the Soil Mechanics and Foundations Division,* vol. 94, pp. 231-253, 1968.

[52] O. B. Andersland and A. G. Douglas, "Soil Deformation Rates and Activation Energies," *Géotechnique,* vol. 20, pp. 1-16, 1970.

[53] T. W. Lambe and R. V. Whitman, *Soil Mechanics*. New York: John Wiley and Sons, 1969.

[54] C. J. R. Coccia and J. S. McCartney, "Thermal volume change of poorly draining

soils I: Critical assessment of volume change mechanisms," *Computers and Geotechnics,* vol. 80, pp. 26-40, 2016.

[55] R. Pusch and N. Güven, "Electron microscopic examination of hydrothermally treated bentonite clay," *Engineering Geology,* vol. 28, pp. 303-314, 1990.

[56] V. Sivakumar, J. G. Doran, and J. Graham, "Particle orientation and its influence on the mechanical behaviour of isotropically consolidated reconstituted clay," *Engineering Geology,* vol. 66, pp. 197-209, 2002.

[57] J. K. Mitchell, D. R. Hooper, and R. G. Campanella, "Permeability of compacted clay," *Journal of the Soil Mechanics and Foundations Division,* vol. 91, pp. 41-65, 1965.

[58] M. M. Allam and A. Sridharan, "The influence of aging on the shear stength behavior of two fine-grained siols," *Canadian Geotechnical Journal,* vol. 16, pp. 391-397, 1979.

[59] H. B. Seed, J. K. Mitchell, and C. K. Chan, "The strength of compacted cohesive soils," in *Research Conference on Shear Strength of Cohesive Soils*, Boulder, Colorado 1960, pp. 877-964.

[60] Y. Tsubakihara and H. Kishida, "Frictional behaviour between normally consolidated clay and steel by two direct shear type apparatuses," *Soil and Foundations,* vol. 33, pp. 1-13, 1993.

[61] D. P. Conduto, *Foundation design principles and paractices*, 2 ed.: Prentice Hall, 2011.

[62] P. W. Mayne and F. H. Kulhawy, "K0-OCR relationships in soil," *Journal of the Geotechnical Engineering Division,* vol. 108, pp. 851-872, 1982.

[63] R. Rajapakse, *Pile Design and Construction Rules of Thumb*, 2 ed.: Elsevier, 2016.

9 Curriculum Vitae: Te-An Wang

EDUCATION

Doctor of Philosophy – Geotechnical Engineering Department of Civil and Environmental Engineering Dissertation Topic: Experimental Study on Side Resistance of Energy Pile in Winter-Mode Operation	University of Wisconsin – Milwaukee (expected June 19th 2020)
Master of Science – Geotechnical Engineering Department of Civil Engineering Thesis: Numerical Analysis on Confinement Effect of Geocells	National Taiwan University, Taiwan (June 2013)
Bachelor of Engineering Department of Civil Engineering	National Cheng Kung University, Taiwan (June 2011)

TEACHING EXPERIENCE

Fall 2018 – Present **Graduate Teaching Assistant – Soil Mechanics, UW – Milwaukee**

Responsible for conducting class twice a week including geotechnical experiments, designing weekly quizzes and final exams, grading assignments and exams, establishing a grading system, serving as the exam proctor, and submitting student academic performance to university counselors.

Fall 2017 – Spring 2018 **Graduate Teaching Assistant – Statics, UW – Milwaukee**

Responsible for teaching class twice a week, designing weekly quizzes and exams, providing students with one-on-one tutoring time, serving as the exam proctor, and establishing a grading system.

FELLOWSHIP

Fall 2015 – Spring 2017 **Graduate Research Assistant, UW – Milwaukee**

Assisted in research project funded by the National Science Foundation. Developed experiment methods. Analyzed results and compilation of reports.

PROFESSIONAL EXPERIENCE

August 2013 – April 2014 **Civil Design Engineer – Gibsin Engineering Ltd., Taiwan**

Deep foundation design and concrete structure design. Analyze survey reports and geologic data, engineering drawings, and estimate quantities and cost of materials and equipment to determine project cost.

AWARDS

Fall 2014 – Spring 2018 **Dean's Doctoral Scholarship, UW – Milwaukee**

A four-year financial package for being support graduate student of outstanding record of scholarly achievement.

December 2016, March 2017, and May 2019 **Chancellor's Graduate Student Award**

Financial support for study in the Civil Engineering PhD program.